iScience

CellPress
OPEN ACCESS

Article

# Substrate stiffness alters layer architecture and biophysics of human induced pluripotent stem cells to modulate their differentiation potential

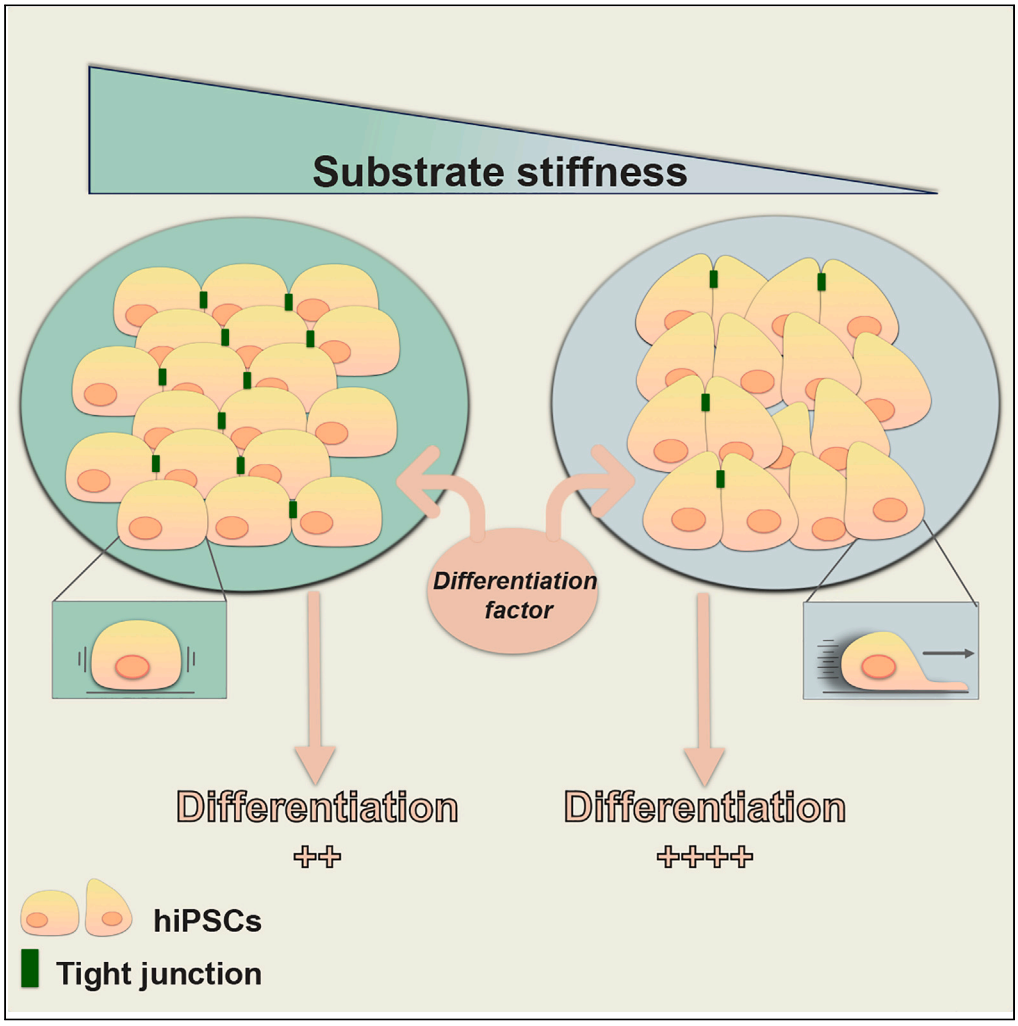


Jack Llewellyn, Anne Charrier, Rossana Cuciniello, Emmanuèle Helfer, Rosanna Dono

rosanna.dono@univ-amu.fr

## Highlights

Tuning of substrate stiffness can enhance mesendoderm/endoderm hiPSC differentiation

Altered tight junction formation drives increased differentiation on soft substrates

Changes in cell motility and interfacial contacts underlie hiPSC layer remodeling

Llewellyn et al., iScience 27, 110557
August 16, 2024 
https://doi.org/10.1016/j.isci.2024.110557

iScience

CellPress
OPEN ACCESS

Article

# Substrate stiffness alters layer architecture and biophysics of human induced pluripotent stem cells to modulate their differentiation potential

Jack Llewellyn,[1,2,3] Anne Charrier,[2] Rossana Cuciniello,[1] Emmanuèle Helfer,[2] and Rosanna Dono[1,4,*]

## SUMMARY

**Lineage-specific differentiation of human induced pluripotent stem cells (hiPSCs) relies on complex interactions between biochemical and physical cues. Here we investigated the ability of hiPSCs to undergo lineage commitment in response to inductive signals and assessed how this competence is modulated by substrate stiffness. We showed that Activin A-induced hiPSC differentiation into mesendoderm and its derivative, definitive endoderm, is enhanced on gel-based substrates softer than glass. This correlated with changes in tight junction formation and extensive cytoskeletal remodeling. Further, live imaging and biophysical studies suggested changes in cell motility and interfacial contacts underlie hiPSC layer reshaping on soft substrates. Finally, we repurposed an ultra-soft silicone gel, which may provide a suitable substrate for culturing hiPSCs at physiological stiffnesses. Our results provide mechanistic insight into how epithelial mechanics dictate the hiPSC response to chemical signals and provide a tool for their efficient differentiation in emerging stem cell therapies.**

## INTRODUCTION

Human pluripotent stem cells (hPSCs), which include human embryonic stem cells (hESCs) and human induced pluripotent stem cells (hiPSCs), are characterized by their ability to self-renew indefinitely in culture while maintaining their ability to differentiate into all human cell types. These properties make them a valuable model system for studies on developmental biology and the genetic basis of diseases as well as for applications in fields such as pharmacology, tissue engineering, and regenerative medicine.[1,2] Much research has been dedicated to exploring methods to induce the differentiation of these cells toward specific lineages by taking advantage of insights gained from developmental biology studies.[3–5]

In embryos, fate and differentiation of PSCs are controlled by a complex interplay of biochemical cues including growth factors, inhibitors, and small bioactive molecules present in their microenvironment.[6–10] For example, inhibition of Nodal/Bone Morphogenetic Protein (BMP) signaling induces neuroectoderm.[8] BMP and Nodal signaling, together with Wingless/Integrated (WNT), are also necessary for mesendoderm differentiation, a common progenitor of definitive mesoderm and definitive endoderm lineages and corresponding to the embryonic primitive streak.[8] Finally, progression from mesendoderm toward either mesoderm or definitive endoderm lineages requires quantitative intercalation of BMP, Nodal, and WNT signals in a precise temporal dynamic.[8] The influence of these biochemical cues has been extensively studied, and standard differentiation protocols *in vitro* mirror developmental stages by the timed addition of these biochemical players. Many experimental studies and computational models have also revealed that hPSCs sense and respond to various physical cues encoded by the microenvironment, such as local forces, cell-cell contacts, and matrix stiffness. With the development of engineering biocompatible substrates and apparatus, the effects of these mechanical stimuli sensed by PSCs in normal developmental processes are currently being tested in order to provide the best approach for the efficient generation of differentiated cells with native properties.

Matrix stiffness, usually characterized by the Young's modulus (one of several different elastic moduli), has emerged as an important physical factor regulating multiple aspects of PSC behavior including division, migration, and differentiation.[11,12] For example, studies on hPSC lineage entry have shown that soft substrates in combination with high mechanical tension enhance hESC mesodermal differentiation.[13,14] Yet, substrates softer than tissue culture polystyrene plates (whose Young's modulus is in the GPa range) induce hESCs and hiPSCs to exit the pluripotency stage and promote spontaneous upregulation of endodermal genes.[15,16] In another study, soft substrates were shown to favor better maintenance of hESC-derived endodermal cells suggesting that control of substrate stiffness might enable a superior control of live cells' endodermal properties.[17] Matrix stiffness, which matches the stiffness of native tissues, can also guide stem cell differentiation towards corresponding tissue lineages. For instance, substrates with Young's moduli close to those of brain (0.1–0.7 kPa), pancreas

[1]Aix Marseille University, CNRS, IBDM, Turing Centre for Living Systems, NeuroMarseille, Marseille, France
[2]Aix Marseille University, CNRS, CINAM, Turing Centre for Living Systems, 13009 Marseille, France
[3]Present address: Royal Veterinary College, University of London, Royal College Street, London, NW1 0TU, GB, UK
[4]Lead contact
*Correspondence: rosanna.dono@univ-amu.fr
https://doi.org/10.1016/j.isci.2024.110557

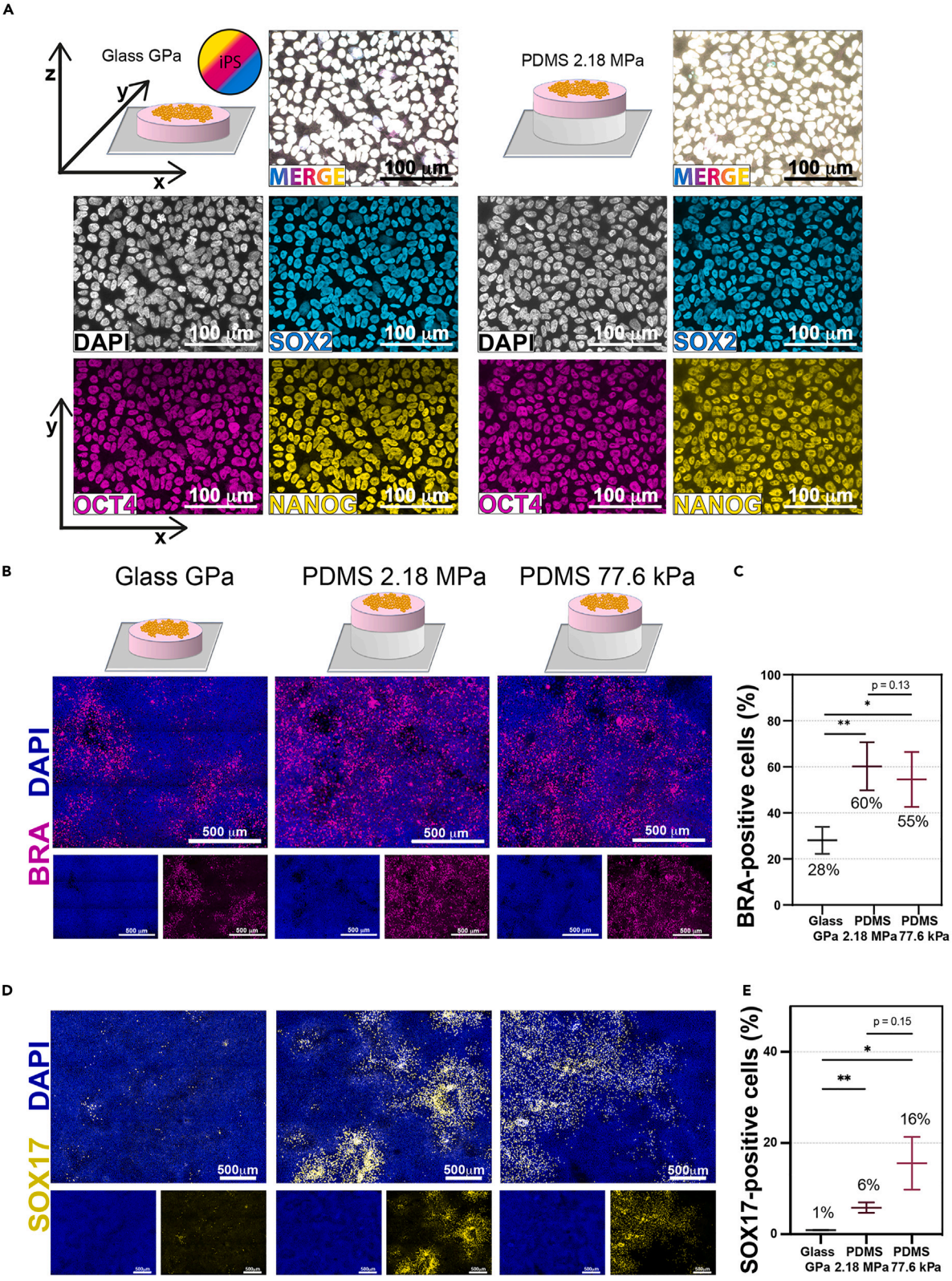
A
Glass GPa
iPS
z
y
x
PDMS 2.18 MPa
MERGE
100 µm
DAPI
SOX2
OCT4
NANOG
B
Glass GPa
PDMS 2.18 MPa
PDMS 77.6 kPa
BRA
DAPI
500 µm
C
BRA-positive cells (%)
p = 0.13
*
**
60%
55%
28%
Glass GPa
PDMS 2.18 MPa
PDMS 77.6 kPa
D
SOX17
DAPI
500µm
E
SOX17-positive cells (%)
p = 0.15
16%
6%
1%

**Figure 1. HiPSCs cultured on functionalized PDMS gel substrates preserve pluripotency while improving the efficiency of early lineage commitment**

(A) Representative immunofluorescence (IF) images of the nuclear marker DAPI and of the pluripotency markers SOX2, OCT4, and NANOG in hiPSCs grown on glass (left) and on PDMS gel of 2.18 MPa stiffness (right). Cells were fixed and images were taken 24 h after the removal of ROCK inhibitor (48 h after cell seeding at 110,000 cells/cm$^2$).

(B) Representative IF images of DAPI and of the mesendoderm marker T-Brachyury (BRA) in hiPSCs grown on glass (left), 2.18 MPa PDMS gel (middle), and 77.6 kPa PDMS gel (right). Cells were fixed and images were taken 24 h after the addition of 100 ng/mL Activin A (48 h after the removal of ROCK inhibitor and 72 h after cell seeding at 110,000 cells/cm$^2$).

(C) Quantification of the number of BRA-positive cells in the three stiffness conditions at the time point illustrated in (B). BRA-positive cells were defined as those whose mean fluorescence intensity was above the 95$^{th}$ percentile of the mean BRA intensity in Activin A-negative control cells at the same time point and stiffness. At least 10 randomly selected frames of view were taken per condition, covering >2.23 mm$^2$ in total. $N = 7$ paired replicates.

(D) Representative IF images of DAPI and of the definitive endoderm marker SOX17 in hiPSCs grown on glass (left), 2.18 MPa PDMS gel (middle), and 77.6 kPa PDMS gel (right). Cells were fixed and images were taken 24 h after the addition of 0.2% fetal bovine serum (FBS; 48 h after the addition of 100 ng/mL Activin A, 72 h after the removal of ROCK inhibitor, and 96 h after cell seeding at 50,000 cells/cm$^2$).

(E) Quantification of the number of SOX17-positive cells in each of the three stiffness conditions at the time point illustrated in (D). SOX17-positive cells were defined via automatic thresholding. At least 3 randomly selected frames of view were taken per condition, covering >21.2 mm$^2$ in total. $N = 4$ unpaired replicates. See also Figures S1, S6, and S7. Scale bar in images, 100 μm (A) and 500 μm (B and D). Data are represented as mean ± SEM, and $p$ values show the results of a two-tailed t test (*, <0.05; **, <0.01).

(1.4–4.4 kPa), muscle (8–17 kPa), and bone tissue (25–40 kPa) direct hPSCs to differentiate into neurons, beta cells, myotubes, and osteoblasts, respectively.[12,18–20] Taken together, these studies suggest that substrate stiffness can provide a tunable parameter to promote PSC lineage entry and differentiation. However, how substrate stiffness interacts with other differentiation-inducing factors, such as biochemical factors, remains largely unclear.

With gradual uncovering of the effect of substrate stiffness on directing cell biological properties, the question of how cells sense their physical microenvironment and make adjustments to control cell function has also raised rapid interest. An emerging concept is that the matrix stiffness is transduced in distinct cell physical features that may be essential for cellular identity and function. For example, differences have been observed in cell spreading or focal adhesion maturation in cells cultured on polydimethylsiloxane (PDMS) substrates compared to rigid glass or tissue culture plates.[21] Consistently, studies on chondrocytes have revealed that soft matrix can induce a reorganization of the actin cytoskeleton enough to efficiently promote chondrocyte differentiation from ATDC5 chondroprogenitor cells.[22] Yet, the elasticity of differentiated chondrocytes increases with matrix stiffness in order to create a homeostatic balance.[23] Similar to chondrocytes, cancer cells also adjust their viscoelasticity in response to changes in extracellular matrix stiffness in order to maintain their invasive phenotypes.[24] Although these and other findings highlight the importance of the biophysical interplay between cells and their microenvironment for cell identity and behavior, these feedback mechanisms remain largely unexplored.

In this study we examined the ability of hiPSCs to acquire a mesendodermal fate in response to mesendoderm-inducing signals, such as Activin A as an *in vitro* surrogate of Nodal, and assessed whether tuning the substrate stiffness can enhance this competence. Our rationale was that modeling this early step of embryonic development *in vitro* could provide the best approach to produce mesendodermal-derived cell types with native properties. We also examined the matrix stiffness-dependent mechanosensing of hiPSCs with a focus on cell's physical properties with the aim of providing a quantitative understanding of the mechanisms that regulate cell interactions with substrates of different stiffness. We showed that hiPSC lineage entry into mesendoderm and its derivative definitive endoderm in response to differentiation triggering factors are enhanced when undifferentiated cells are exposed to gel-based substrates with stiffnesses lower than that of standard glass supports. This correlated with changes in the dynamics of tight junction (TJ) formation and with an extensive remodeling of the actin cytoskeleton. Moreover, live imaging in combination with manipulation of the cell mechanoenvironment revealed that the biophysical mechanisms underlying the enhanced differentiation potential of these hiPSCs exposed to softer substrates may rely on distinct cell motility and less influential cell-cell contacts. Given that some hiPSC lines do not grow on ultra-soft polyacrylamide (PA) gels, our results also provide evidence that mechanically buffered silicone matrices can provide a suitable alternative for expansion and differentiation of hiPSCs on ultra-soft substrates. Our studies, by providing new knowledge of matrix stiffness-dependent biological and biophysical behavior of hiPSCs, have important implications for optimization of matrix material and for advancing hiPSC-based clinical applications.

## RESULTS

### Efficiency of hiPSC lineage entry is cell matrix stiffness dependent

To evaluate whether matrix stiffness regulates hiPSC self-renewal and mesendodermal cell fate, we cultured hiPSCs on substrates of different stiffness. We fabricated substrates made of thin (50–100 μm thick), flat silicone gels (PDMS) deposited on glass coverslips via high-speed spin coating. The Young's modulus of these PDMS gels can be tuned by varying the base:catalyst (PDMS:crosslinker) ratio in the silicone mixture. We used four ratios of 90:10, 95:5, 96:4, and 98:2, leading to different stiffnesses, with Young's modulus extreme values of 2.18 MPa and 77.6 kPa for the 90:10 and 98:2 ratios, respectively (see "Gel compositions and corresponding Young's moduli" in STAR methods). All PDMS stiffnesses were much lower than that of glass, which is in the GPa range. Both PDMS gel layers and glass support were coated with Matrigel to promote hiPSC attachment in a similar way. We first examined whether changes in matrix stiffness affect hiPSC self-renewal by analyzing the expression of pluripotency markers. Immunocytochemistry analysis of SOX2, OCT4, and NANOG proteins revealed that all cells remained positive for and maintained high expression levels of these pluripotency genes regardless of substrate stiffness (glass and

PDMS 2.18 MPa; Figure 1A). Analysis of OCT4 and of the epithelial marker E-Cadherin (E-CAD) showed unchanged expression levels across a large range of matrix stiffnesses going from that of glass (of the order of the GPa) to that of the least reticulated PDMS gel (98:2 base:catalyst, 77.6 kPa), suggesting that changes in substrate stiffness do not perturb expression of pluripotency genes (Figure S1A). We thus focused on the two gels with the highest and lowest stiffnesses for further experiments. Interestingly, quantitative analysis of cell confluency over time suggests an increase in cell density for cultures grown on PDMS gels compared to glass (Figures S1B and S1C; see STAR methods).

Next, we tested the response of hiPSCs to the signal Activin A, an *in vitro* surrogate of Nodal, commonly used to trigger mesendoderm differentiation.[25–29] 24 h following the addition of 100 ng/mL Activin A to the culture medium, we quantified the competence of cells to acquire a mesendodermal fate when exposed to different matrix stiffnesses by analyzing the mesendoderm marker T-Brachyury (BRA). Immunocytochemistry revealed that the number of BRA-positive cells increased by 2-fold in cells grown on PDMS gels compared to glass (Figures 1B and 1C; percentage of BRA-positive cells: glass 28.1% ± 5.8%; PDMS 2.18 MPa: 60.3% ± 10.4%; PDMS 77.6 kPa: 54.5% ± 11.9%). Interestingly, while significantly more BRA-expressing cells were seen when comparing either PDMS gel versus glass, no significant difference was seen between the two PDMS gels.

To investigate whether this increased differentiation efficiency in hiPSCs cultured on matrices softer than glass is maintained as mesendodermal cells acquire an endodermal fate, we applied a minimal endoderm differentiation protocol by culturing mesendodermal cells only in the presence of Activin A (instead of Activin A and the GSK3 inhibitor CHIR99021[30]) and of defined heat-inactivated 0.2% fetal bovine serum (FBS) for an additional 24 h and determined the extent of definitive endoderm by using the marker SOX17. Of note, a significant increase in the number of SOX17-positive cells was observed in the differentiating cells cultured on both PDMS gels compared to glass, which we quantified as at least a 6-fold increase in SOX17-positive cells (Figures 1D and 1E; percentage of SOX17-positive cells: glass 0.8% ± 0.1%; PDMS 2.18 MPa: 5.7% ± 1.2%; PDMS 77.6 kPa: 15.5% ± 5.8%). This quantitative analysis also revealed a tendency for cells grown on the 77.6 kPa PDMS gel to differentiate more efficiently into endodermal cells than those grown on the 2.18 MPa PDMS gel, thus suggesting a positive correlation between softer substrates and competence to become endodermal cells.

The PDMS-silicone base utilized in the experiments described earlier (Figure 1) is well-documented and commonly used for cell culture applications; however, a consistently reported lower limit of the base:catalyst ratio restricts its use to study cell differentiation efficiency at very low stiffnesses <1 kPa.[12,31,32] In previous studies of mammalian cell behavior on ultra-soft substrates, PA hydrogels have been commonly used. We therefore investigated the differentiation of hiPSCs on PA hydrogel substrates, similarly coated with Matrigel like PDMS gels and glass. Similar to PDMS gels, PA mixtures of acrylamide and bis-acrylamide were prepared at varying ratios to fabricate PA hydrogel of varying stiffnesses, with Young's moduli of 2.15, 4.07, 11.60, 25.10, and 32.10 kPa (see "Gel compositions and corresponding Young's moduli" in STAR methods). In agreement with previous studies of hiPSCs/hESCs,[33–35] we found that our hiPSCs did not grow as a 2D epithelium at PA stiffnesses below 10 kPa and preferentially formed 3D aggregates (Figure S2A) even in the presence of increasing concentrations of Matrigel or by gradually decreasing matrix stiffness to favor adaptation of cells to the new environment. Therefore, we concluded that the use of PA hydrogels was not compatible with studies of matrix stiffness effects on differentiation of our hiPSC line for Young's modulus values below 10 kPa.

PDMS gels and PA hydrogels have distinct chemistry, which could potentially affect the differentiation properties of hiPSCs. However, all substrates (glass, silicon gels, and PA hydrogels) were coated with Matrigel to promote cell attachment to the surface. As a result, the surface chemistry was expected to be the same for all experiments and to not impact the cell behavior. To confirm this, hiPSCs were grown on PDMS gel and PA hydrogel of comparable stiffnesses versus glass and differentiation efficiency was quantified. Cells underwent similar mesendoderm differentiation as assessed by the presence of BRA-positive cells (Figure S2B), and, as expected, we did not observe any difference in differentiation efficiency (Figure S2C; percentage of BRA-positive cells: glass: 19% ± 0.4%; PDMS 38 kPa: 1.1% ± 6%; PA 11.6 kPa: 39% ± 2.8%).

Taken together, these results show that substrates with a lower stiffness than glass are compatible with expansion of hiPSCs and efficient differentiation into mesendoderm. As the 2-fold increase of mesendoderm-positive cells translates into a 6-fold increase into SOX17-positive cells as differentiation proceeds (see the number of SOX17-positive cells in hiPSCs differentiated on PDMS gels), it is likely that an exposure of hiPSCs to soft matrices at the lineage entry point amplifies the capability of differentiating cells to pursue the later differentiation steps.

## Epithelial and cytoskeletal organization is modulated by substrate stiffness

Previously, we have shown that the strength of the hiPSC response to Activin A and the differentiation efficiency into the mesendoderm lineage can be enhanced by disrupting hiPSC epithelial integrity revealed by using the TJ protein Zona Occludens 1 (ZO1) to map cell-cell contacts and discriminate areas of organized epithelial structure with well-defined and regular ZO1 cell junctions from those with abnormal TJ organization.[36] To understand whether changes in matrix stiffness alter the hiPSC epithelial layer, we used the same approach. 24 h after the removal of Rho kinase inhibitor (ROCK inhibitor)—the time point at which Activin A was introduced in differentiation assays—cells exhibited a reasonable organized epithelial structure on the glass substrate. In contrast, we found a significant higher loss of epithelial integrity in hiPSCs grown on both PDMS gels, whether of 2.18 MPa or 77.6 kPa stiffnesses (Figure 2A). Moreover, quantitative analysis revealed similar levels of disorganization independently of the PDMS gel stiffness (Figure 2B; percentage of ZO1 organization: glass 67% ± 7%; PDMS 2.18 MPa: 52% ± 8%; PDMS 77.6 kPa: 49% ± 6%). Similarly, comparing glass with PDMS gel and PA hydrogel of stiffnesses of the same order, we found that a similar loss of epithelial integrity characterizes both gel types (Figures S2D and S2E; percentage of surface covered by ZO1-bounded cells: glass 91% ± 1%; PDMS 77.6 kPa 83% ± 3%; PA 32 kPa 82% ± 1%).

Of note, analysis of epithelial integrity by ZO1 immunostaining at later time points of 48 and 72 h after ROCK inhibitor removal revealed a progressive reorganization of the epithelial cell layer in hiPSCs cultured on PDMS gels with an establishment of TJs to nearly 100% after 72 h (Figure S3). This result indicates that reducing matrix stiffness causes a delay in TJ formation rather than preventing this cell-cell interaction.

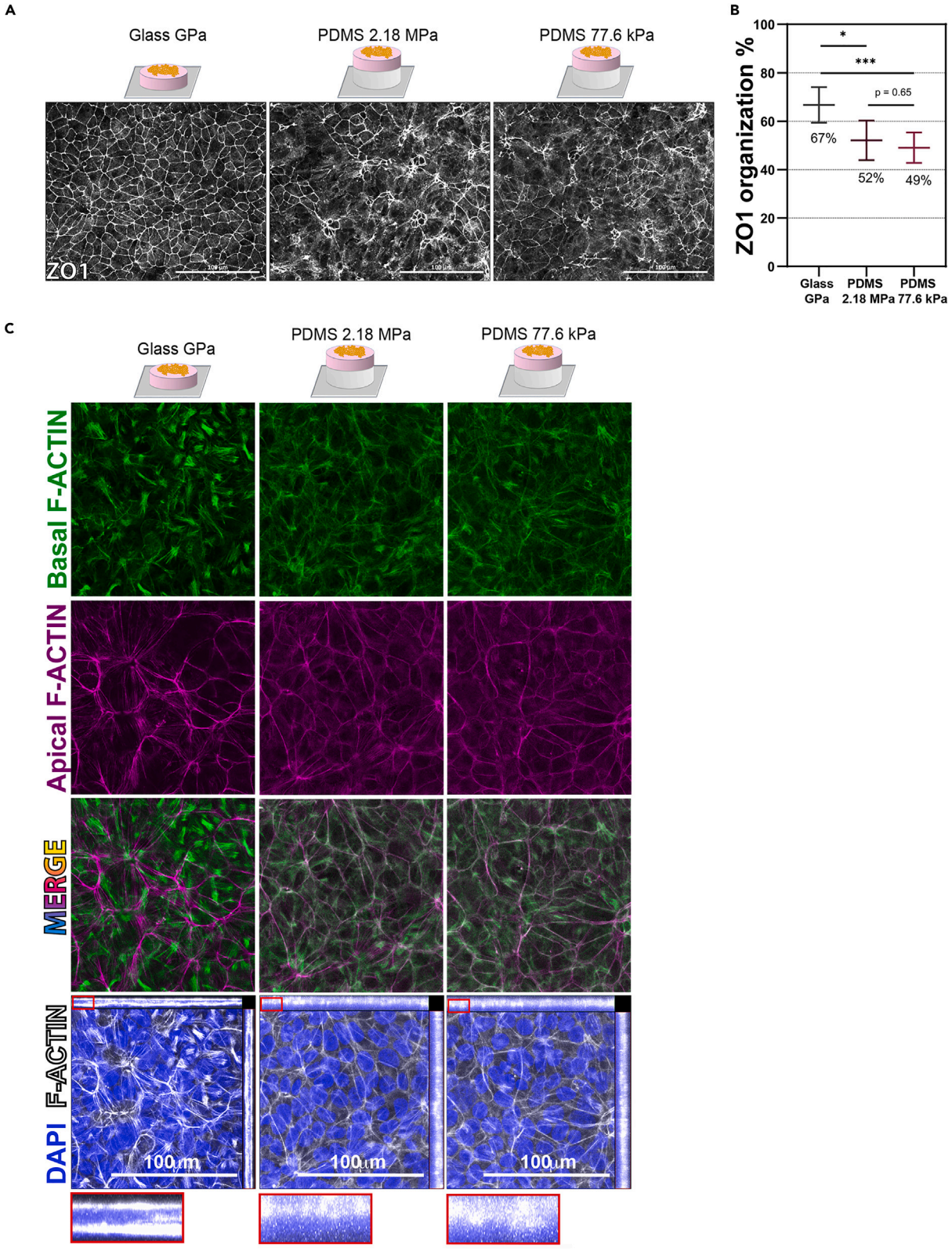
A
Glass GPa
PDMS 2.18 MPa
PDMS 77.6 kPa
ZO1
B
ZO1 organization %
100
80
60
40
20
0
*
***
p = 0.65
67%
52%
49%
Glass GPa
PDMS 2.18 MPa
PDMS 77.6 kPa
C
Glass GPa
PDMS 2.18 MPa
PDMS 77.6 kPa
Basal F-ACTIN
Apical F-ACTIN
MERGE
DAPI F-ACTIN
100 µm
100 µm
100 µm

**Figure 2. Epithelial and cytoskeletal organization of hiPSCs is perturbed on PDMS gel substrates**

(A) Representative IF images of the tight junction protein ZO1 in hiPSCs grown on glass (left), 2.18 MPa PDMS gel (middle), and 77.6 kPa PDMS gel (right). Cells were fixed and images were taken 24 h after the removal of ROCK inhibitor (48 h after cell seeding at 110,000 cells/cm$^2$).

(B) Quantification of the ZO1 organization in the three stiffness conditions at the time point illustrated in (A). ZO1 organization was defined as the percentage of the frame of view covered by ZO1-bounded cells. Areas of ZO1-bounded cells were detected automatically. At least 3 randomly selected frames of view were taken per condition, covering >5.28 mm$^2$ in total. $N = 6$ ratio paired replicates.

(C) Representative IF images of the nuclear marker DAPI and of phalloidin iFluor 647-labeled F-ACTIN in hiPSCs grown on glass (left), 2.18 MPa PDMS gel (middle), and 77.6 kPa PDMS gel (right). Cells were fixed and images were taken 24 h after the removal of ROCK inhibitor (48 h after cell seeding at 110,000 cells/cm$^2$). Shown in green (first row) and magenta (second row) are the x-y planes of basally and apically located actin cortex, respectively, detected automatically. In the bottom row (x-y, x-z, and y-z planes) and red insert (magnified x-z plane), maximum intensity projections of actin across all planes are shown. See also Figures S2–S7. Scale bars in all images, 100 μm. Data are represented as mean ± SEM, and $p$ values show the results of a two-tailed t test (*, <0.05; **, <0.01; ***, <0.001).

Having demonstrated that differentiation efficiency is increased and epithelial integrity is reduced on gels versus glass, we next sought to determine whether other chemical and physical aspects of the gel-based substrates could cause these cellular organization changes. First, PDMS gels are naturally hydrophobic, in contrast with glass and PA hydrogels. The two PDMS gels were plasma activated in order to reverse their surface hydrophobicity and make them hydrophilic. hiPSCs were plated on plasma-activated gels versus non-activated gels and glass and immunostained for ZO1. Image analysis at 24 h post-seeding revealed impaired TJ formation in hiPSCs plated on plasma-activated gels to a similar extent as non-activated gels (Figure S4A) showing that PDMS hydrophobicity does not affect the Matrigel coating. Second, we investigated the potential impact of the gel surface roughness. Indeed, the PDMS gels' thin layers are prepared via spin coating of liquid droplets of base:catalyst mixtures, followed by an overnight incubation at 60°C to induce reticulation. This method is expected to produce a smooth gel surface topography similar to that of glass.[16] This was confirmed by atomic force microscopy (AFM) measurements that showed that the gel roughness was less than 0.5 nm (Figure S4B; average roughness: PDMS 2.18 MPa: 0.16 nm; PDMS 77.6 kPa: 0.32 nm), even smaller than that of glass, which is of the order of 5 nm. We thus conclude that the PDMS gel surface topography is comparable to that of glass, with no impact on TJ formation.

Taken together, these results point to substrate stiffness as the dominant factor in determining the TJ organization of the hiPSC epithelial layer as surface chemistry or topography is not affected by the nature of the gel.

As changes in cell matrix and cell-cell contacts are known to remodel the cellular cytoskeleton,[14] we examined the distribution of the ACTIN cytoskeleton, namely the actin cortex which is made of actin filaments (F-ACTIN), in hiPSCs grown on the two PDMS gels of different stiffnesses versus hiPSCs grown on glass. Analysis of F-ACTIN localization demonstrated the occurrence of an ACTIN cytoskeleton remodeling in cells on PDMS gels when compared to glass (Figure 2C). In particular, on glass, there was a markedly increased presence of basal stress fibers when compared to PDMS gels, where concentrated ACTIN fibers were mostly apico-lateral (Figure 2C). Z-projections of F-ACTIN on the three substrates further emphasized this remodeling (Figure 2C, red insert).

## Stiffness-mediated control of cell differentiation relies on epithelial organization

As discussed earlier, disruption of the epithelial integrity in hiPSCs increases their differentiation potential in mesendoderm and definitive endoderm by promoting accessibility to Activin A receptors otherwise masked by a tight TJ assembly.[36] In line with our previous report, analysis of mesendoderm differentiated hiPSCs, grown on glass and two PDMS gels and immunostained for ZO1 and BRA, revealed a notable localization of BRA-positive cells near areas of altered ZO1 organization (Figure 3C top). Therefore, we next assessed whether disruption of the epithelial integrity in hiPSCs grown on gels could underlie their increased differentiation potential into mesendoderm and definitive endoderm. This was addressed by using the same approach we reported in Legier et al.,[36] namely restoring the epithelial integrity in hiPSCs using lysophosphatidic acid (LPA), a small molecule known to accelerate epithelial organization and the formation of cell contacts through swelling of the apical membrane.[37] A 24-h treatment of hiPSCs grown on both PDMS gels with 5 μM LPA was sufficient to promote TJ organization and epithelial integrity of cells to levels comparable to those of cells grown on glass (almost fully organized following LPA treatment; Figures 3A and 3B). Consistent with an increase of TJ organization of hiPSCs on PDMS gels, their differentiation efficiency was reduced to the same level as that of hiPSCs on glass upon LPA treatment (Figure 3C), as estimated by the quantitative analysis of BRA-positive cells (Figure 3D; percentage of BRA-positive cells upon Activin A treatment: glass 28.1% ± 5.8%; PDMS 2.18 MPa: 60.3% ± 10.4%; PDMS 77.6 kPa: 54.5% ± 11.9%; percentage of BRA-positive cells upon Activin A and LPA treatment: glass 2.4% ± 0.5%; PDMS 2.18: MPa 5.5% ± 2.6%; PDMS 77.6 kPa: 3.8% ± 1.8%). Interestingly, the BRA-positive cells in the LPA-treated differentiating cells localized to areas of disrupted ZO1 organization (Figure 3C). In conclusion, LPA treatment resulted into a drastic reduction of the differentiation efficiency of hiPSCs independently of substrate stiffness (nearly 0% in all conditions).

LPA, in addition to its role in apical membrane swelling, appears to directly regulate multiple aspects of hPSC pluripotency and differentiation, ranging from upregulation of gene expression during lineage-specific differentiation (e.g., BRA expression in mesoderm induction) to inhibition of hESC differentiation, as in the differentiation of hESC-derived neural stem cells (SCs) into neurons.[38–40] We therefore asked whether the observed reduction in mesendoderm differentiated cells upon LPA treatments might simply be due to a direct LPA-mediated inhibition of the mesendoderm differentiation process. Uncoupling the potential indirect effects of LPA on hiPSC differentiation through apical membrane swelling from the direct effect of LPA on the regulation of hiPSC differentiation is rather problematic, as epithelial organization through the formation of TJ-mediated cell-cell contacts is concomitant to the reduction in the number of differentiated cells. To circumvent

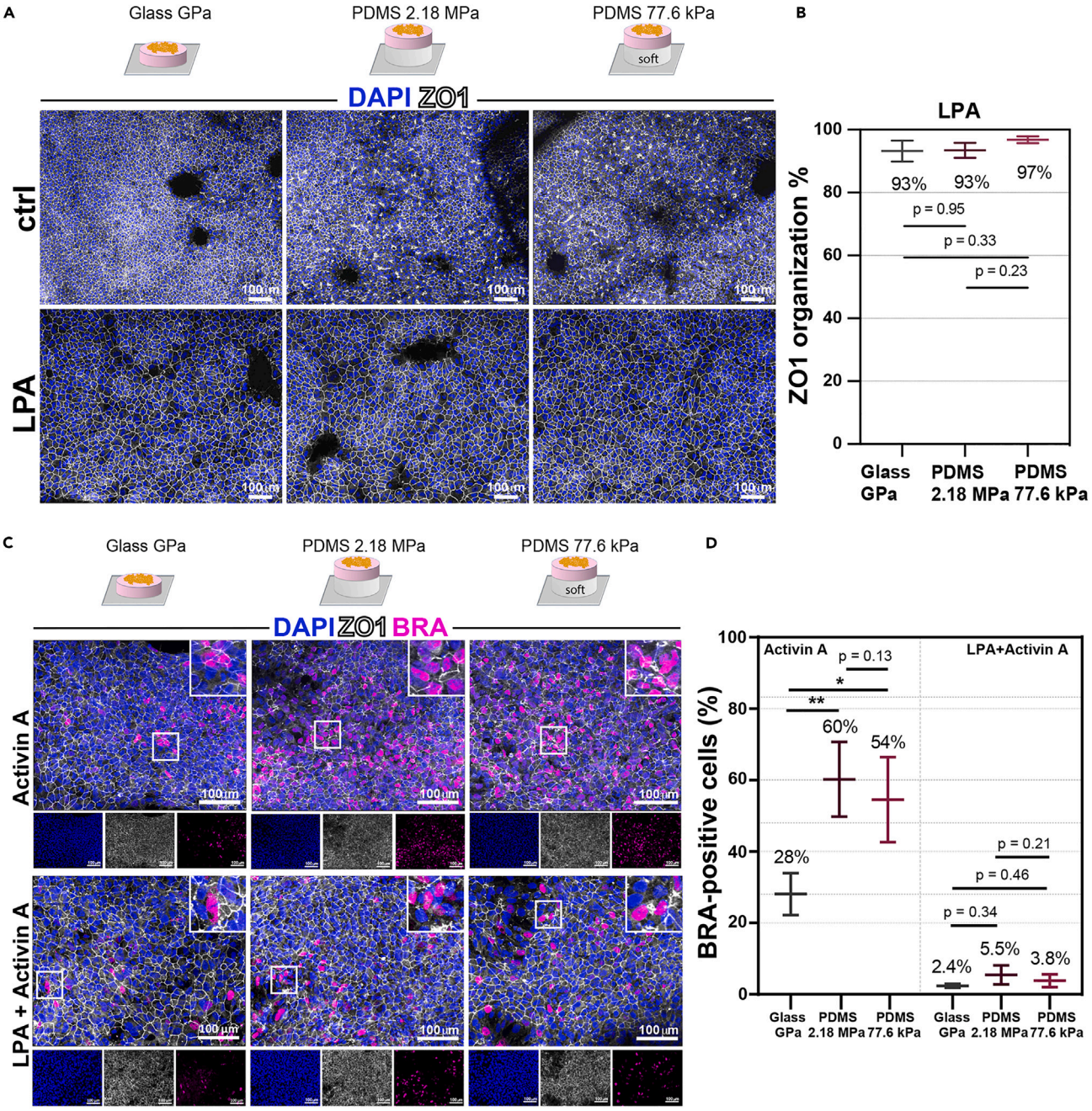


**Figure 3. Substrate stiffness controls early lineage commitment in hiPSCs via a mechanism dependent on epithelial disorganization**

(A) Representative IF images of the nuclear marker DAPI and of the tight junction protein ZO1 in hiPSCs grown on glass (left), 2.18 MPa stiffness PDMS gel (middle), and 77.6 kPa stiffness PDMS gel (right). 6 h after cell seeding, ROCK inhibitor was removed and either blank (top) or 5 μM lysophosphatidic acid (LPA, bottom), was added to the culture media. Cells were fixed and images were taken 24 h after the removal of ROCK inhibitor (30 h after cell seeding at 130,000 cells/cm$^2$).

(B) Quantification of the ZO1 organization in the three stiffness conditions in the presence of LPA. ZO1 organization was defined as the percentage of the frame of view covered by ZO1-bounded cells. Areas of ZO1-bounded cells were detected automatically. At least 5 randomly selected frames of view were taken per condition, covering >4.40 mm$^2$ in total. $N = 1$, with error bars representing the variance across frames of view.

(C) Representative IF images of DAPI, ZO1, and the mesendoderm marker BRA in hiPSCs grown on glass (left), 2.18 MPa stiffness PDMS gel (middle), and 77.6 kPa stiffness PDMS gel (right). White squares indicate the position of enlargements shown in each panel. Cells were fixed and images were taken 24 h after the addition of 100 ng/mL Activin A (48 h after the removal of ROCK inhibitor, addition or not of 5 μM LPA, and 72 h after cell seeding at 110,000 cells/cm$^2$).

**Figure 3. *Continued***

(D) Quantification of the number of BRA-positive cells in the three stiffness conditions, in the absence (panels Activin A) and in the presence of LPA (panels LPA + Activin A) at the time point illustrated in (C). BRA-positive cells were defined as those whose mean fluorescence intensity was above the 95th percentile of the mean BRA intensity in Activin A-negative control cells at the same time point and stiffness. At least 10 randomly selected frames of view were taken per condition, covering >2.23 $mm^2$ in total. $N = 3$ paired replicates.

See also Figures S5–S7. Scale bars in all images, 100 μm. Data are represented as mean ± SEM, and $p$ values show the results of a two-tailed t test (*, <0.05; **, <0.01).

this obstacle and gain additional insight into the role of epithelial integrity in hiPSC differentiation potential, we used mesendoderm differentiated cultures (without LPA) on glass to quantify the percentage of BRA-positive cells in ZO1-organized versus ZO1-disorganized areas. The results showed a striking positive correlation between higher numbers of BRA-positive cells and areas of disrupted ZO1 organization (Figure S5A; percentage of BRA-positive cells upon Activin A treatment: ZO1-organized areas 31.7% ± 8.9%; ZO1-disorganized areas 61.1% ± 5.6%). To corroborate this finding, we next performed cell differentiation studies in cells undergoing progressive reorganization of the epithelial cell layer, as revealed by ZO1 immunostaining (Figure S3). To this end, differentiation induced by Activin A treatment was initiated at 24, 48, and 56 h after ROCK inhibitor removal. Consistent with an increase in TJ organization, the differentiation efficiency of hiPSCs in the mesendoderm and definitive endoderm was reduced, as shown by the decrease distribution of BRA- and SOX17-positive cells between 24 and 56 h (Figure S5B). Notably, differentiated cells were mainly found in ZO1-disorganized areas similar to what was observed before and after LPA treatment, meaning that LPA by itself does not impact the localization of differentiated cells to disorganized areas.

Taken together, these results indicate that an impaired TJ organization in hiPSCs cultured on gels may be the cellular/tissue mechanism that promotes enhanced differentiation, thus indicating a key role for epithelial organization in the stiffness-mediated control of cell differentiation.

## Ultra-soft silicone provides a reliable alternative to study hiPSC differentiation

Given that hiPSCs preferentially form 3D aggregates on ultra-soft PA hydrogels (<10 kPa), we tested a different type of silicone gel, named QGel, more commonly used in electronics and much less-documented within biological sciences, whose stiffness can be tuned down to very low values in the kPa range.[41] Utilizing the same method as for the former PDMS-based substrates, i.e., spin coating base:catalyst mixture droplets of varying ratios onto glass coverslips, we fabricated QGel-based thin substrates with three stiffnesses of 31.2, 1.9, and below 1.9 kPa, which was the limit of detection for stiffness measurement (see "Gel compositions and corresponding Young's moduli" in STAR methods). We next tested whether hiPSCs were able to attach and grow on these ultra-soft QGels, coated with Matrigel. In contrast to ultra-soft PA hydrogels with a Young's modulus of 2.15 kPa, hiPSCs reliably formed a 2D epithelium on the QGel softer than 1.9 kPa (Figure 4A). As with the other silicone gels, the ultra-soft QGels did not affect hiPSC self-renewal, as revealed by retained expression of the pluripotency markers NANOG, OCT4, and SOX2 (Figure 4B). Notably, cells cultured on ultra-soft QGels exhibited a similar perturbation of epithelial organization as seen on the softest PDMS gel (77.6 kPa) when compared to glass (Figures 4C and 4B; percentage of surface covered by ZO1-bounded cells: glass 49% ± 7%; PDMS 77.6 kPa 29% ± 4%; QGel <1.9 kPa 27% ± 5%).

Next, we tested the differentiation ability of hiPSCs on QGels by triggering endoderm lineage entry. As shown by the analysis of SOX17-positive cells, hiPSCs grown on QGels show increased differentiation efficiency when compared to hiPSCs grown on glass (Figures 4E and 4F; percentage of SOX17-positive cells: glass 4.2% ± 1.1%; PDMS 77.6 kPa 20.2% ± 2.7%; QGel <1.9 kPa 23.2% ± 0.4%). Moreover, differentiation level of hiPSCs on the softest QGel was comparable to that on the 77.6-kPa PDMS gel thus showing that QGels replicate loss of TJ organization and increased differentiation efficiency of hiPSCs on substrates softer than glass. In conclusion, our results show that QGel ultra-soft matrices are compatible with expansion and differentiation of hiPSCs, with cell behavior similar to that seen using more common silicone substrates. In this way, QGels provide a new substrate to test the effects of ultra-soft gels with stiffnesses lower than 10 kPa for cell lines, like some hiPSC lines, which are not compatible with ultra-soft PA hydrogels.

## Epithelial structures point to an increased fluidity of hiPSC colonies on softer substrates

Having found that cells grown on PDMS/QGel silicone gels and PA hydrogels show a disruption of epithelial integrity versus cells grown on glass, we next sought to decipher whether this phenotype correlates with changes of hiPSC physical properties in response to matrix stiffness. We first performed live imaging of cells growing on the soft PDMS gel (77.6 kPa), on the ultra-soft QGel (<1.9 kPa), and on glass over 6 h and examined both single cells and colonies, 0–6 h and 24–30 h after the removal of ROCK inhibitor, respectively (glass versus PDMS: Videos S1, S2, S3, and S4; glass versus QGel: Videos S5, S6, S7, and S8). We measured the correlation coefficient between frames from these time lapses. This coefficient quantifies how different a video frame is compared to the preceding one, i.e., how much cells have globally moved between the two frames. This approach averages all cell movements over a large field of view within a single analysis step and allows measurement of the mean global motility over time. In contrast with the tracking of individual cells which requires statistics over hundreds of cells to reduce the impact of high heterogeneity within a cell population, the correlation coefficient smoothens the population heterogeneity and highlights differences in motility purely due to environmental conditions. This allowed us to quantify how the motility of hiPSCs changes on gel substrates compared to glass, both outside (single cells) and inside of colonies.[42–44] Though very close, the correlation coefficients over 6 h-periods are significantly different at both selected time windows between glass and PDMS (Figure 5A, left; correlation coefficient 0–6 h: glass GPa 0.8556 ± 0.0013, PDMS 77.6 kPa 0.8471 ± 0.0022; correlation coefficient 24–30 h: glass GPa 0.8944 ± 0.0011, PDMS 77.6 kPa 0.8862 ± 0.0009) and between glass and QGel (Figure 5A, right; correlation coefficient 0–6 h: glass GPa 0.9206 ± 0.0008, QGel 0.8819 ± 0.00022;

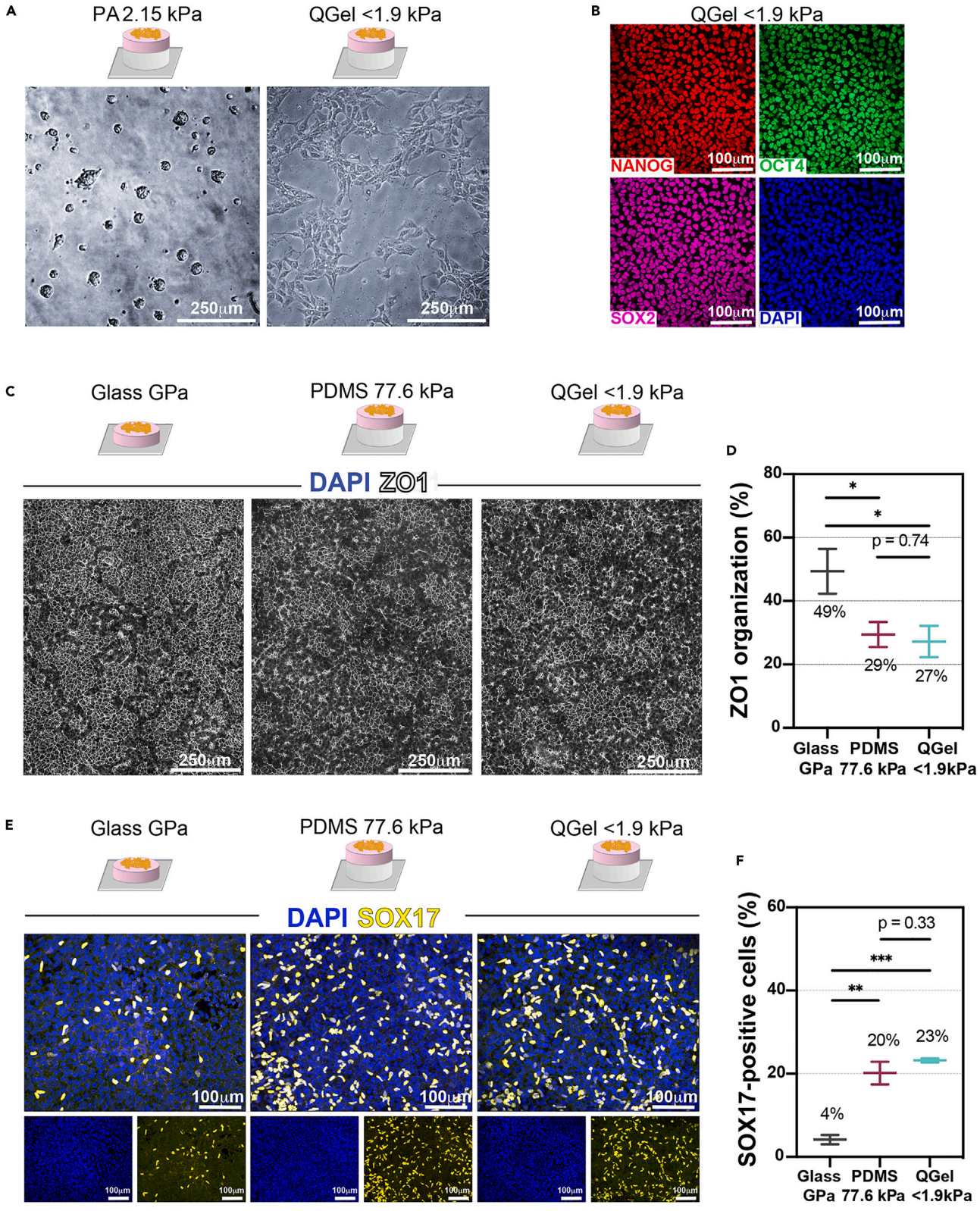
A
PA 2.15 kPa
QGel <1.9 kPa
250μm
250μm
B
QGel <1.9 kPa
NANOG
100μm
OCT4
100μm
SOX2
100μm
DAPI
100μm
C
Glass GPa
PDMS 77.6 kPa
QGel <1.9 kPa
DAPI ZO1
250μm
250μm
250μm
D
ZO1 organization (%)
80
60
40
20
0
*
*
p = 0.74
49%
29%
27%
Glass GPa
PDMS 77.6 kPa
QGel <1.9kPa
E
Glass GPa
PDMS 77.6 kPa
QGel <1.9 kPa
DAPI SOX17
100μm
100μm
100μm
F
SOX17-positive cells (%)
60
40
20
0
p = 0.33
***
**
20%
23%
4%
Glass GPa
PDMS 77.6 kPa
QGel <1.9kPa

**Figure 4. QGels permit expansion and differentiation of hiPSCs on ultra-soft substrates**

(A) Bright-field images of the inability/ability of hiPSCs to adhere and grow as a 2D epithelium on 2.15 kPa PA hydrogels (left) and on <1.9 kPa QGel (right). Cells were fixed and images were taken 24 h after cell seeding at 110,000 cells/cm$^2$.

(B) Representative IF images of the nuclear marker DAPI and of the pluripotency markers NANOG, OCT4, and SOX2 in hiPSCs grown on QGel <1.9 kPa. Cells were fixed and images were taken 24 h after the removal of ROCK inhibitor (48 h after cell seeding at 110,000 cells/cm$^2$).

(C) Representative IF images of the tight junction protein ZO1 in hiPSCs grown on glass (left), soft PDMS gel (77.6 kPa, middle), and ultra-soft QGel (<1.9 kPa, right). Cells were fixed and images were taken 24 h after the removal of ROCK inhibitor (48 h after cell seeding at 110,000 cells/cm$^2$).

(D) Quantification of the ZO1 organization in the three stiffness conditions at the time point illustrated in (C). ZO1 organization was defined as the percentage of the frame of view covered by ZO1-bounded cells. Areas of ZO1-bounded cells were detected automatically. At least 4 randomly selected frames of view were taken per condition, covering >7.04 mm$^2$ in total. $N$ = 4 unpaired replicates. Note that hiPSCs plated on glass displayed approximately 50%–70% of TJ organization in different experiments depending on the growth rate of cells at the plating stage (compare Figures 4D and 2B).

(E) Representative IF images of the nuclear marker DAPI and of the definitive endoderm marker SOX17 in hiPSCs grown on glass (left), 77.6 kPa PDMS gel (middle), and <1.9 kPa QGel (right). Cells were fixed and images were taken 24 h after the addition of 0.2% FBS (48 h after the addition of 100 ng/mL Activin A, 72 h after the removal of ROCK inhibitor, and 96 h after cell seeding at 50,000 cells/cm$^2$).

(F) Quantification of the number of SOX17-positive cells in each of the three stiffness conditions at the time point illustrated in (E). SOX17-positive cells were defined via automatic thresholding. At least 3 randomly selected frames of view were taken per condition, covering >21.2 mm$^2$ in total. $N$ = 3 unpaired replicates. See also Figures S6 and S7. Scale bars in images, 250 μm (A and C) and 100 μm (B and E). Data are represented as mean ± SEM, and $p$ values show the results of a two-tailed t test (*, <0.05; **, <0.01; ***, <0.001).

correlation coefficient 24–30 h: glass 0.7901 ± 0.0011, QGel 0.7618 ± 0.0010). This shows that cells growing on PDMS gel and QGel, either as single cells or colonies, are more motile when compared to cells growing on glass.

Next, we analyzed how the epithelial structure of hiPSCs differs on substrates of high, low, and very low stiffnesses (glass versus soft PDMS 77.6 kPa versus ultra-soft QGel <1.9 kPa; Figure 4C). To do so, we compared representative regions of epithelia at 24 h following ROCK inhibitor removal, displaying both organized and disorganized areas identified via ZO1 immunostaining[36] in the three stiffness conditions. Epithelial tissue architecture is known to relate to cell packing,[45] so we first examined the cell density in the organized and disorganized areas (Figure 5B). On the three substrates, cells are less dense in disorganized areas (Figures 5B and 5C; cell density in cells/mm$^2$: organized: glass GPa 6,309 ± 121.8, PDMS 77.6 kPa 6,063 ± 155.6; QGel <1.9 kPa 6,007 ± 208.7; disorganized: glass GPa 5,384 ± 155.6, PDMS 77.6 kPa 5,405 ± 220.7; QGel <1.9 kPa 4,884 ± 224.5). Moreover, cell density showed a general downtrend with decreasing substrate stiffness. As both substrate stiffness and cell organization can affect cell density, we performed a multiple variable statistical test to discriminate each effect, which showed that the cell density tends to be lower on the soft substrates with a significant decrease for QGel (Figure 5C).

We then sought to identify a parameter linked to cell mechanical features. We thus analyzed the shape index of cells in the three epithelia focusing on ZO1-organized regions (Figure 5D). This shape index, defined as the cell perimeter divided by the square root of the cell area, illustrates the competition between cell cortical tension and cell-cell contacts that both affect the cell shape. In cell layers with strong epithelial organization, a lower shape index indicates that cortical tension dominates the cell shape, whereas a higher shape index indicates that cell-cell adhesion has a stronger influence on cell shape.[43] In our study, hiPSC layers are much more disorganized than typically dense monolayers, and we used the shape index to estimate differences in the impact of cell-cell adhesion at the time point used to trigger differentiation. We found that the shape index of cells progressively decreased with substrate stiffness (Figure 5E; glass: 4.59 ± 0.025; PDMS 4.546 ± 0.026; QGel 4.467 ± 0.028), suggesting more influential cell-cell contacts on stiffer substrates for our hiPSC structures. To note, all shape index values are much higher than 3.81, the threshold value of a solid-like jammed tissue,[43] which indicates that our hiPSCs layers are in a fluid-like state whatever the substrate, but with a decreasing impact of cell-cell contacts on the softer substrates.

Together, the results of the live imaging analysis and cell shape index suggest that the epithelial organization of cells within colonies on stiffer substrates is less fluid, due to lower cell motility, and that cells are tightly connected with high interfacial tension. In contrast, on softer substrates, the increased motility of cells leads to more fluid colonies with less influential cell-cell contacts and, consequently, a slower rate of epithelial organization.

## DISCUSSION

Understanding the mechanisms behind mammalian lineage commitment remains a considerable challenge, especially in human embryos. The prevailing idea is that crosstalk between biochemical and physical cues regulates the early processes of embryonic development. HPSCs, serving as *in vitro* models of the human epiblast, offer a unique opportunity to dissect these intricate processes while permitting independent manipulation of the underlying mechanisms. In the present study, we have explored whether the competence of hiPSCs to undergo mesendoderm and definitive endoderm differentiation in response to Activin A stimulation can be modulated by altering substrate stiffness as the selected physical cue. We demonstrated that differentiation of hiPSCs along these lineages can be improved when hiPSCs are cultured on substrates softer than glass, such as PDMS/QGel silicone gels and PA hydrogels with stiffnesses ranging between a few MPa and a few kPa, which are far below the GPa stiffness of glass. Of note, hiPSCs cultured on these gels exhibit alterations in TJ formation and a disrupted epithelial integrity. Furthermore, cells are more motile and exhibit a decrease of their shape index that suggests cell-cell contacts have less influence on the epithelial structure. These phenotypes cause a delay in TJ formation kinetics, which is the basis of the increased differentiation potential of hiPSCs on gels, as demonstrated by rescue and differentiation time course experiments. Thus, the results of this study provide a mechanistic insight into how physical inputs from the microenvironment modify the epithelial properties of hiPSCs, which ultimately determine their response to differentiation triggering biochemical signals.

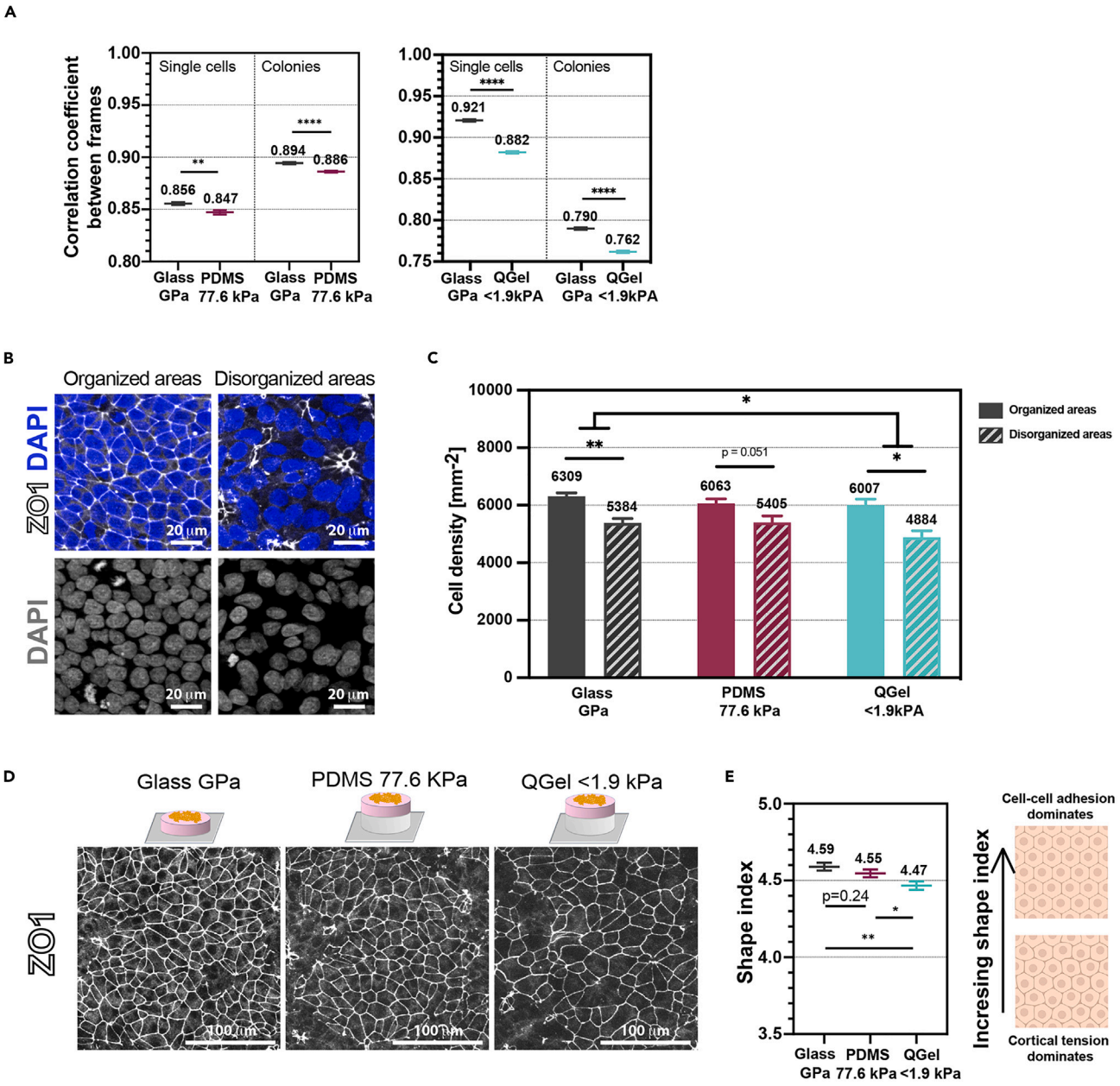


**Figure 5. HiPSCs growing on gel substrates are more motile, less dense, and with less influential cell-cell adhesion**

(A) Quantification of the correlation coefficients between successive frames of the videos shown in Videos S1, S2, S3, and S4 (glass versus 77.6 kPa PDMS, left) and Videos S5, S6, S7, and S8 (glass versus <1.9 kPa QGel, right). An automatic mask was used to remove non-cell areas from each frame, and arrays representing the frames were subjected to a 2D correlation analysis. Frames were taken with a 5 min time interval over 6 h, giving $N = 72$ pairs of successive frames in each condition.

(B) Representative IF images of the nuclei, using the nuclear marker DAPI, in ZO1-organized and disorganized areas, illustrating the decrease in cell density under disrupted epithelial organization. The displayed regions are 100×100 $\mu m^2$.

(C) Quantification of the cell density in ZO1-organized and disorganized areas on GPa glass, soft 77.6 kPa PDMS gel, and ultra-soft <1.9 kPa QGel. The nucleus counting was used as a proxy for cell counting. ZO1-organized areas were detected automatically, and ZO1-disorganized areas were determined as the complementary areas in the images. Nuclei were automatically detected and counted in each area. At least 3 randomly selected frames of view were taken per condition covering >1.31 $mm^2$ in total. $N = 4$ unpaired replicates.

(D) Magnified regions of epithelia taken from the data quantified in Figure 4C, showing hiPSCs grown on glass (left), 77.6 kPa PDMS gel (middle), and <1.9 kPa QGel (right) with similar percentages of ZO1 organization.

**Figure 5. *Continued***

(E) (Left) quantification of the shape index in each of the three images in (D). The shape index is defined as the cell perimeter divided by the square root of the cell area. Cells were segmented automatically using the Tissue Analyzer algorithm, and cell perimeter and area were measured using FIJI. (Right) illustration of the epithelial phenotype of shape index that reports the balance between cortical tension and cell-cell adhesion.

See also Figure S7. Scale bars in images, 20 μm (B) and 100 μm (D). Data are represented as mean ± SEM, and *p* values show the results of a two-tailed t test (*, <0.05; **, <0.01; ***, <0.001; ****, <0.0001). For (C), a two-tailed t test was used to compare cell density between organized and disorganized areas in the three substrate conditions and a multiple variable test was used to compare cell density between the three substrate conditions (*, <0.05; **, <0.01).

Recent research indicates that the TJ scaffolding protein ZO1, which connects the TJ transmembrane proteins to the cytoskeleton,[46] plays a role in regulating TJ assembly that is in part dependent on tension.[47] Notably, the mechanical forces acting on ZO1 depend on extracellular matrix stiffness.[48] This implies that ZO1 may help create junctions by adapting the cytoskeletal forces generated in the cell body to the developing TJs. In support of this are our results showing a broad cytoskeletal remodeling on substrates softer than glass, with a striking loss of basal ACTIN. Substrate stiffness is well known to impact cell adhesion to the surface, and motility has been thoroughly investigated at the single-cell level,[49] but the consequences on cell epithelial assembly are less understood. Here, the alteration of ACTIN basal structures may impact its overall organization and consequently the associated ZO1 cell-cell connections. In addition, our cell shape analysis showed that the cortical tension, generated by the actin cortex, becomes more dominant over the interfacial forces generated by the TJs. Based on these findings, substrate stiffness has an impact on TJ formation that may depend on cytoskeletal interactions with ZO1. Further research is required to determine whether these changes are associated with specific mechanical tension on ZO1, and whether this tension is only due to actin fibers.

Correlated with the altered organization, we observed a lower packing of the cells compared to organized areas, consistent with destabilized TJs. More importantly, we also observed an overall lower cell density on the soft substrates compared to glass, regardless of the degree of organization. This lower density may be related to a looser epithelial organization due to higher cell motility. Our live-imaging analysis shows that hiPSC cells, whether single at early times after seeding or in colonies at later times after cell proliferation, exhibit higher motility levels on soft silicone gels. Such increased motility may explain the impaired epithelial integrity we observed compared to glass: more motile cells on soft substrates may cause a delay in the stabilization of cell-cell contacts after cell dissociation and seeding. Overall, our results are consistent, showing a lower cell density with less tightly bound and more motile cells, leading to increased cell layer fluidity and a delay in epithelial organization. Future work on signal perception in epithelial tissues should seek to further quantify how the mechanoenvironment affects cell layer fluidity. In addition, our results suggest that the balance between cortical tension and cell-cell contacts is altered when substrate stiffness is changed, but complementary assays should be performed to quantify this change, e.g., whether both tension and adhesion are altered, or only one is increased or decreased while the other is unchanged.

Through our rescue experiments, we present evidence that the kinetics of TJ formation play a crucial role in the regulation of hiPSC fate acquisition in response to differentiation factors. As per our previous findings, the loss of morphogen regulator GLYPICAN-4 in hiPSCs causes disruption in epithelial integrity with areas of TJ formation being affected.[36] This phenotype results in the Activin A receptors being exposed to the culture medium, thereby enhancing hiPSCs' capacity to detect Activin A and maintain activation of the Activin A pathway over a prolonged period. This situation results in an enhanced differentiation potential into mesendoderm and definitive endoderm lineages. Based on these results, we hypothesize that hiPSCs on gels develop greater competence in perceiving the Activin A differentiation signal due to areas of disrupted TJs in which receptors might be more exposed, resulting in more efficient differentiation. Additionally, it is also likely that a modification in the fluidity of hiPSC colonies on gels (as mentioned earlier) increases Activin A receptor accessibility across the entire hiPSC layer, leading to improved Activin A signal perception. Crucially, our rescue of epithelial organization ceased differentiation in response to Activin A almost entirely in all conditions. This demonstrates that the stiffness-mediated effect on cells' sensitivity to Activin A signaling depends on the effects of stiffness on epithelial organization.

Interestingly, this disruption of epithelial integrity for hiPSCs grown on gels does not perturb self-renewal or the expression of pluripotency genes nor promotes premature expression of mesendoderm, endoderm, or other lineage markers (present study and in previous studies[36,50]). Thus, substrate stiffness-dependent alterations in TJs alone do not appear sufficient to promote differentiation or determine lineage fate choices. The observed maintenance of stemness/pluripotency of hiPSCs grown on gels is consistent with previous studies from Przybyla et al. and Guo et al. showing that changes in the PA hydrogel stiffness ranging from 60 kPa to 0.4 kPa and 3.5 kPa, respectively, do not affect these biological properties of hESCs.[14,17] Interestingly, while Przybyla et al. found increased levels of B-catenin, E-CAD, and P120-cadherin at cell junctions in hESCs on a 0.4-kPa gel, perhaps indicative of more developed junctions between cells, we find here a loss of ZO1—more apically located along the cell junction—on similarly soft substrates.[14] Further, our finding of increased cell motility on gels is in agreement with the finding of Przybyla et al. that hESCs on softer substrates experience weaker cell-ECM adhesion.[14] Notably, Guo et al. found that hESCs grown on a 0.4-kPa PA hydrogel underwent a significant change in shape, resulting in colonies with a rounded morphology similar to those we observed in our study with hiPSCs grown on PA hydrogels with stiffnesses lower than 10 kPa.[17] Contrary to the previously mentioned outcomes, Musah et al. discovered that utilizing a soft PA hydrogel with a Young's modulus around 0.7 kPa causes downregulation of pluripotency genes while promoting neuronal lineage entry and differentiation into post-mitotic neurons, even if the cells are grown in a self-renewing medium.[51] Similarly, Chen et al. demonstrated that using soft PA hydrogels with stiffnesses of 3, 15, and 33 kPa causes downregulation of pluripotency genes and primes hiPSC differentiation toward the endoderm lineage, without requiring endoderm induction medium.[15] Unfortunately, it was not reported in these two studies if the hPSCs grown on these soft PA-based substrates maintain their epithelial morphology or develop a spherical colony shape, which could impact their behavior. While designing substrates to bypass the need for

differentiation-inducing factors is fascinating, the aforementioned studies also suggest that different hPSC lines could react differentially to substrate stiffness. In particular, on soft PA-based substrates with similar stiffnesses (0.4 kPa[14] and around 0.7 kPa[51]), hPSCs can retain stemness and pluripotency[14] or develop into neuronal lineages.[51] These findings also suggest that additional unknown factors present in culture conditions might cooperate with substrate stiffness in the establishment of hPSC behavior, which could have implications for a reproducible lineage acquisition and maintenance. We suggest that identifying the optimal substrate stiffness to preserve pluripotency in hPSCs, while enhancing differentiation potential under differentiation conditions, could prevent such variations. This would enable precise control of culture conditions for cell therapy, disease modeling, and bio-mechanistic studies.

Our research here and others' findings indicate that PA hydrogels with stiffness lower than 10 kPa may not always support the maintenance of hiPSC epithelial morphology. A common reasoning is that cells will preferentially form 3D aggregates and detach (present studies and previous studies[34,35]). Our experiments, using QGels of varying stiffness down to less than 2 kPa, indicate that this kind of substrate should enable the maintenance of self-renewal and pluripotency of hPSCs for which ultra-soft PA hydrogel is not compatible for growth and maintenance in an undifferentiated state. The QGel silicone gels are frequently utilized in electronics as they provide protection against moisture, vibration, and thermal or mechanical shock. While the material has been used sporadically as an ultra-soft substrate to study cell mechanobiology,[41,52–54] here we present for the first time its suitability for hPSC culture and studies of cell differentiation in physiological stiffness conditions. We hypothesize that hiPSCs and hESCs may be particularly sensitive to vibrations during cell culture, which is exacerbated on ultra-soft substrates. Our findings reveal that silicone QGels are innovative materials that allow for the culture and differentiation of hPSCs, without inducing any adverse effects, when combined with bioactive molecules like Matrigel.

Additionally, QGels seem to offer some technical advantages compared to PA hydrogel. Traditional PA hydrogel layers are most commonly fabricated by sandwiching the liquid gel mixture between glass surfaces[55]; however silicone gels are sufficiently viscous to enable droplet spin coating onto glass coverslips, which allows for more precise and reliable control of gel properties such as thickness and surface smoothness. Further, the dependence of PA hydrogels on initiators (ammonium persulfate and N,N,N,N-tetramethylethylendiamine (TEMED)) introduces batch variance in gel polymer lengths and elasticity (https://www.bio-rad.com/webroot/web/pdf/lsr/literature/Bulletin_1156.pdf). It has also been shown that cells are less able to form stable focal adhesions on ultra-soft PA hydrogels, due to the marked porosity of these gels.[56,57] We thus hypothesize that the adhesion, buffering, and elasticity features of QGel silicone gels facilitate the adhesion and growth of hPSCs, which are otherwise unsuitable for culture on ultra-soft but porous substrates like PA hydrogels.

In conclusion, our work highlights that, by optimizing the mechanical properties of the extracellular substrate, hPSCs can be maintained in a self-renewing pluripotent state, and mesendoderm as well as definitive endoderm differentiation can be enhanced. We also provide evidence of the mechanism underlying the enhanced differentiation potential of hiPSCs grown on gels by showing that substrate stiffness-triggered changes in the epithelial cell layer architecture can facilitate sensing of signaling proteins. Therefore, our study offers a crucial new and original perspective to several reports of "optimal" stiffnesses for hiPSC differentiation which neglect to analyze the epithelial cell layer organization. We expect that this mechanism will be of more general relevance in other hPSC lineage entry processes and differentiation events. Similar to several other studies, we find conventional and easily available gel materials unsuitable for studying hiPSCs at ultra-soft stiffnesses (<10 kPa). By repurposing a silicone encapsulant more common to the field of electronics, we circumvent this lower limit and show that these phenotypes persist at physiological stiffnesses. The interdisciplinary nature of our research provides novel perspectives on how cells combine physical and biological cues to initiate crucial processes, emphasizing the significance of investigating the function of composite interfaces in development, physiology, and pathology.

### Limitations of the study

In this study, our focus was on the impact of matrix stiffness on differentiation of one hiPSC line into mesendoderm and endoderm lineages, and we revealed the underlying cellular mechanisms that drive this differentiation. It remains to be verified if TJ disruption, triggered by decrease of the matrix stiffness, also affects mesendoderm and endoderm differentiation in other hiPSC lines as well as the neuroectoderm and mesoderm differentiation, which will be explored in the future.

Our biophysical analysis of epithelial organization suggested that on soft substrates cell-cell interactions become dominated by cortical tension. This change in the competition between these two features needs to be confirmed by quantitative approaches which were not in the scope of this study: for example, laser ablation of the tissue would allow to measure the stress relaxation, from which one can derive the anisotropy and the amplitude of the interfacial stress. Moreover, ablation in organized and disorganized areas within the same tissue will allow to decipher in a quantitative way how the balance between tension and adhesion is modulated between these areas.

## STAR★METHODS

Detailed methods are provided in the online version of this paper and include the following:

- KEY RESOURCES TABLE
- RESOURCE AVAILABILITY
  - Lead contact
  - Materials availability
  - Data and code availability
- EXPERIMENTAL MODEL AND STUDY PARTICIPANT DETAILS

## SUPPLEMENTAL INFORMATION

Supplemental information can be found online at https://doi.org/10.1016/j.isci.2024.110557.

## ACKNOWLEDGMENTS

We thank all members of our labs for helpful discussions and comments, L. Fasano and M. Merkel for critical reading of the manuscript, T. Legier and E. Bazellières for discussions and reagents, T. Legier and T. Boudier for image analysis pipelines and macros, T. Duong Quoc Le for assistance with video analysis, and C. Guijarro-Calvo and W. Kong for assistance with Tissue Analyzer algorithms. Microscopy was performed at the imaging platform of the IBDM, supported by the ANR through the "Investments for the Future" program (France-BioImaging, ANR-10-INSB-04-01). The authors thank the members of the IBDM core facility for microscopy for their technical support. The IBDM is affiliated to NeuroMarseille, the AMU neuroscience network, and to NeuroSchool, the AMU graduate school in neuroscience supported by the A*MIDEX foundation (AMX-19-IET-004) and the "Investissements d'Avenir" program (nEURo*AMU, ANR-17-EURE-0029 grant). E.H. belongs to the French Consortium Approches Quantitatives du Vivant/Quantitative Approaches to Living Systems (AQV). The project leading to this publication has received funding from Excellence Initiative of Aix-Marseille University - A*MIDEX (A-*M*-AAP-ID-17-66-170301-11.30) and from France 2030, the French Government program managed by the French National Research Agency (ANR-16-CONV-0001). This work was also funded by France Parkinson (Convention 2021-239736), Fondation de France (2023-265613), Fondation Louis Justin Besançon, and COEN Pathfinder III (Network of Centres of Excellence in Neurodegeneration; COEN4014) to R.D. The funders had no role in the study design, data collection and analysis, decision to publish, or preparation of the manuscript.

## AUTHOR CONTRIBUTIONS

Conceptualization, J.L., E.H., and R.D.; methodology, J.L. and R.D.; investigation, J.L., A.C., R.C., E.H., and R.D.; writing – original draft, J.L. and R.D.; writing – review and editing, J.L., A.C., R.C., E.H., and R.D.; funding acquisition, E.H. and R.D.; supervision, E.H. and R.D.

## DECLARATION OF INTERESTS

The authors declare no competing interests.

Received: February 1, 2024
Revised: June 10, 2024
Accepted: July 17, 2024
Published: July 19, 2024

## REFERENCES

1. Avior, Y., Sagi, I., and Benvenisty, N. (2016). Pluripotent stem cells in disease modelling and drug discovery. Nat. Rev. Mol. Cell Biol. *17*, 170–182. https://doi.org/10.1038/nrm.2015.27.
2. Yamanaka, S. (2020). Pluripotent Stem Cell-Based Cell Therapy-Promise and Challenges. Cell Stem Cell *27*, 523–531. https://doi.org/10.1016/j.stem.2020.09.014.
3. Chen, K.G., Mallon, B.S., Johnson, K.R., Hamilton, R.S., McKay, R.D.G., and Robey, P.G. (2014). Developmental insights from early mammalian embryos and core signaling pathways that influence human pluripotent cell growth and differentiation. Stem Cell Res. *12*, 610–621. https://doi.org/10.1016/j.scr.2014.02.002.
4. Keller, G. (2005). Embryonic stem cell differentiation: emergence of a new era in biology and medicine. Genes Dev. *19*, 1129–1155. https://doi.org/10.1101/gad.1303605.
5. Nelson, C.M. (2022). Mechanical Control of Cell Differentiation: Insights from the Early Embryo. Annu. Rev. Biomed. Eng. *24*,

307–322. https://doi.org/10.1146/annurev-bioeng-060418-052527.
6. Arnold, S.J., and Robertson, E.J. (2009). Making a commitment: cell lineage allocation and axis patterning in the early mouse embryo. Nat. Rev. Mol. Cell Biol. *10*, 91–103. https://doi.org/10.1038/nrm2618.
7. Brennan, J., Lu, C.C., Norris, D.P., Rodriguez, T.A., Beddington, R.S., and Robertson, E.J. (2001). Nodal signalling in the epiblast patterns the early mouse embryo. Nature *411*, 965–969. https://doi.org/10.1038/35082103.
8. Rivera-Pérez, J.A., and Hadjantonakis, A.K. (2014). The Dynamics of Morphogenesis in the Early Mouse Embryo. Cold Spring Harb. Perspect. Biol. *7*, a015867. https://doi.org/10.1101/cshperspect.a015867.
9. Tam, P.P.L., and Loebel, D.A.F. (2007). Gene function in mouse embryogenesis: get set for gastrulation. Nat. Rev. Genet. *8*, 368–381. https://doi.org/10.1038/nrg2084.
10. Zhang, Z., Zwick, S., Loew, E., Grimley, J.S., and Ramanathan, S. (2019). Mouse embryo geometry drives formation of robust signaling gradients through receptor localization. Nat. Commun. *10*, 4516. https://doi.org/10.1038/s41467-019-12533-7.
11. Gerardo, H., Lima, A., Carvalho, J., Ramos, J.R.D., Couceiro, S., Travasso, R.D.M., Pires das Neves, R., and Grãos, M. (2019). Soft culture substrates favor stem-like cellular phenotype and facilitate reprogramming of human mesenchymal stem/stromal cells (hMSCs) through mechanotransduction. Sci. Rep. *9*, 9086. https://doi.org/10.1038/s41598-019-45352-3.
12. Evans, N.D., Minelli, C., Gentleman, E., LaPointe, V., Patankar, S.N., Kallivretaki, M., Chen, X., Roberts, C.J., and Stevens, M.M. (2009). Substrate stiffness affects early differentiation events in embryonic stem cells. Eur. Cell. Mater. *18*, 1–14. , discussion 13-14. https://doi.org/10.22203/ecm.v018a01.
13. Muncie, J.M., Ayad, N.M.E., Lakins, J.N., Xue, X., Fu, J., and Weaver, V.M. (2020). Mechanical Tension Promotes Formation of Gastrulation-like Nodes and Patterns Mesoderm Specification in Human Embryonic Stem Cells. Dev. Cell *55*, 679–694.e11. https://doi.org/10.1016/j.devcel.2020.10.015.
14. Przybyla, L., Lakins, J.N., and Weaver, V.M. (2016). Tissue Mechanics Orchestrate Wnt-Dependent Human Embryonic Stem Cell Differentiation. Cell Stem Cell *19*, 462–475. https://doi.org/10.1016/j.stem.2016.06.018.
15. Chen, Y.F., Li, Y.S.J., Chou, C.H., Chiew, M.Y., Huang, H.D., Ho, J.H.C., Chien, S., and Lee, O.K. (2020). Control of matrix stiffness promotes endodermal lineage specification by regulating SMAD2/3 via lncRNA LINC00458. Sci. Adv. *6*, eaay0264. https://doi.org/10.1126/sciadv.aay0264.
16. Eroshenko, N., Ramachandran, R., Yadavalli, V.K., and Rao, R.R. (2013). Effect of substrate stiffness on early human embryonic stem cell differentiation. J. Biol. Eng. *7*, 7. https://doi.org/10.1186/1754-1611-7-7.
17. Guo, A., Wang, B., Lyu, C., Li, W., Wu, Y., Zhu, L., Bi, R., Huang, C., Li, J.J., and Du, Y. (2020). Consistent apparent Young's modulus of human embryonic stem cells and derived cell types stabilized by substrate stiffness regulation promotes lineage specificity maintenance. Cell Regen. *9*, 15. https://doi.org/10.1186/s13619-020-00054-4.
18. Jiwlawat, N., Lynch, E.M., Napiwocki, B.N., Stempien, A., Ashton, R.S., Kamp, T.J., Crone, W.C., and Suzuki, M. (2019). Micropatterned substrates with physiological stiffness promote cell maturation and Pompe disease phenotype in human induced pluripotent stem cell-derived skeletal myocytes. Biotechnol. Bioeng. *116*, 2377–2392. https://doi.org/10.1002/bit.27075.
19. Keung, A.J., Asuri, P., Kumar, S., and Schaffer, D.V. (2012). Soft microenvironments promote the early neurogenic differentiation but not self-renewal of human pluripotent stem cells. Integr. Biol. *4*, 1049–1058. https://doi.org/10.1039/c2ib20083j.
20. Narayanan, N.K., Duan, B., Butcher, J.T., Mazumder, A., and Narayanan, B.A. (2014). Characterization of multiple myeloma clonal cell expansion and stromal Wnt/beta-catenin signaling in hyaluronic acid-based 3D hydrogel. In Vivo *28*, 67–73.
21. Petzold, J., and Gentleman, E. (2021). Intrinsic Mechanical Cues and Their Impact on Stem Cells and Embryogenesis. Front. Cell Dev. Biol. *9*, 761871. https://doi.org/10.3389/fcell.2021.761871.
22. Allen, J.L., Cooke, M.E., and Alliston, T. (2012). ECM stiffness primes the TGFbeta pathway to promote chondrocyte differentiation. Mol. Biol. Cell *23*, 3731–3742. https://doi.org/10.1091/mbc.E12-03-0172.
23. Zhang, T., Gong, T., Xie, J., Lin, S., Liu, Y., Zhou, T., and Lin, Y. (2016). Softening Substrates Promote Chondrocytes Phenotype via RhoA/ROCK Pathway. ACS Appl. Mater. Interfaces *8*, 22884–22891. https://doi.org/10.1021/acsami.6b07097.
24. Wullkopf, L., West, A.K.V., Leijnse, N., Cox, T.R., Madsen, C.D., Oddershede, L.B., and Erler, J.T. (2018). Cancer cells' ability to mechanically adjust to extracellular matrix stiffness correlates with their invasive potential. Mol. Biol. Cell *29*, 2378–2385. https://doi.org/10.1091/mbc.E18-05-0319.
25. Cermola, F., D'Aniello, C., Tatè, R., De Cesare, D., Martinez-Arias, A., Minchiotti, G., and Patriarca, E.J. (2021). Gastruloid Development Competence Discriminates Different States of Pluripotency. Stem Cell Rep. *16*, 354–369. https://doi.org/10.1016/j.stemcr.2020.12.013.
26. D'Amour, K.A., Agulnick, A.D., Eliazer, S., Kelly, O.G., Kroon, E., and Baetge, E.E. (2005). Efficient differentiation of human embryonic stem cells to definitive endoderm. Nat. Biotechnol. *23*, 1534–1541. https://doi.org/10.1038/nbt1163.
27. Hayes, K., Kim, Y.K., and Pera, M.F. (2021). A case for revisiting Nodal signaling in human pluripotent stem cells. Stem Cell. *39*, 1137–1144. https://doi.org/10.1002/stem.3383.
28. Laflamme, M.A., Chen, K.Y., Naumova, A.V., Muskheli, V., Fugate, J.A., Dupras, S.K., Reinecke, H., Xu, C., Hassanipour, M., Police, S., et al. (2007). Cardiomyocytes derived from human embryonic stem cells in pro-survival factors enhance function of infarcted rat hearts. Nat. Biotechnol. *25*, 1015–1024. https://doi.org/10.1038/nbt1327.
29. Turner, D.A., Girgin, M., Alonso-Crisostomo, L., Trivedi, V., Baillie-Johnson, P., Glodowski, C.R., Hayward, P.C., Collignon, J., Gustavsen, C., Serup, P., et al. (2017). Anteroposterior polarity and elongation in the absence of extra-embryonic tissues and of spatially localised signalling in gastruloids: mammalian embryonic organoids. Development *144*, 3894–3906. https://doi.org/10.1242/dev.150391.
30. Kreuser, U., Buchert, J., Haase, A., Richter, W., and Diederichs, S. (2020). Initial WNT/beta-Catenin Activation Enhanced Mesoderm Commitment, Extracellular Matrix Expression, Cell Aggregation and Cartilage Tissue Yield From Induced Pluripotent Stem Cells. Front. Cell Dev. Biol. *8*, 581331. https://doi.org/10.3389/fcell.2020.581331.
31. Ahmed, N., Murosaki, T., Kakugo, A., Kurokawa, T., Gong, J.P., and Nogata, Y. (2011). Long-term observation of barnacle growth on soft substrates with different elasticity and wettability. Soft Matter *7*, 7281–7290. https://doi.org/10.1039/c1sm05483j.
32. Yang, H.W., Liu, X.Y., Shen, Z.F., Yao, W., Gong, X.B., Huang, H.X., and Ding, G.H. (2018). An investigation of the distribution and location of mast cells affected by the stiffness of substrates as a mechanical niche. Int. J. Biol. Sci. *14*, 1142–1152. https://doi.org/10.7150/ijbs.26738.
33. Musah, S., Morin, S.A., Wrighton, P.J., Zwick, D.B., Jin, S., and Kiessling, L.L. (2012). Glycosaminoglycan-binding hydrogels enable mechanical control of human pluripotent stem cell self-renewal. ACS Nano *6*, 10168–10177. https://doi.org/10.1021/nn3039148.
34. Paiva, S., Joanne, P., Migdal, C., Soler, E.L., Hovhannisyan, Y., Nicolas, A., and Agbulut, O. (2020). Polyacrylamide Hydrogels with Rigidity-Independent Surface Chemistry Show Limited Long-Term Maintenance of Pluripotency of Human Induced Pluripotent Stem Cells on Soft Substrates. ACS Biomater. Sci. Eng. *6*, 340–351. https://doi.org/10.1021/acsbiomaterials.9b01189.
35. Price, A.J., Huang, E.Y., Sebastiano, V., and Dunn, A.R. (2017). A semi-interpenetrating network of polyacrylamide and recombinant basement membrane allows pluripotent cell culture in a soft, ligand-rich microenvironment. Biomaterials *121*, 179–192. https://doi.org/10.1016/j.biomaterials.2016.12.005.
36. Legier, T., Rattier, D., Llewellyn, J., Vannier, T., Sorre, B., Maina, F., and Dono, R. (2023). Epithelial disruption drives mesendoderm differentiation in human pluripotent stem cells by enabling TGF-beta protein sensing. Nat. Commun. *14*, 349. https://doi.org/10.1038/s41467-023-35965-8.
37. Medelnik, J.P., Roensch, K., Okawa, S., Del Sol, A., Chara, O., McHedlishvili, L., and Tanaka, E.M. (2018). Signaling-Dependent Control of Apical Membrane Size and Self-Renewal in Rosette-Stage Human Neuroepithelial Stem Cells. Stem Cell Rep. *10*, 1751–1765. https://doi.org/10.1016/j.stemcr.2018.04.018.
38. Blauwkamp, T.A., Nigam, S., Ardehali, R., Weissman, I.L., and Nusse, R. (2012). Endogenous Wnt signalling in human embryonic stem cells generates an equilibrium of distinct lineage-specified progenitors. Nat. Commun. *3*, 1070. https://doi.org/10.1038/ncomms2064.
39. Dottori, M., Leung, J., Turnley, A.M., and Pébay, A. (2008). Lysophosphatidic acid inhibits neuronal differentiation of neural stem/progenitor cells derived from human embryonic stem cells. Stem Cell. *26*, 1146–1154. https://doi.org/10.1634/stemcells.2007-1118.
40. Xu, F., Deng, C., Ren, Z., Sun, L., Meng, Y., Liu, W., Wan, J., and Chen, G. (2021). Lysophosphatidic acid shifts metabolic and transcriptional landscapes to induce a distinct cellular state in human pluripotent

stem cells. Cell Rep. *37*, 110063. https://doi.org/10.1016/j.celrep.2021.110063.

41. Wahl, A., Dinet, C., Dillard, P., Nassereddine, A., Puech, P.H., Limozin, L., and Sengupta, K. (2019). Biphasic mechanosensitivity of T cell receptor-mediated spreading of lymphocytes. Proc. Natl. Acad. Sci. USA *116*, 5908–5913. https://doi.org/10.1073/pnas.1811516116.
42. Fodor, É., Mehandia, V., Comelles, J., Thiagarajan, R., Gov, N.S., Visco, P., van Wijland, F., and Riveline, D. (2018). Spatial Fluctuations at Vertices of Epithelial Layers: Quantification of Regulation by Rho Pathway. Biophys. J. *114*, 939–946. https://doi.org/10.1016/j.bpj.2017.12.026.
43. Lenne, P.F., and Trivedi, V. (2022). Sculpting tissues by phase transitions. Nat. Commun. *13*, 664. https://doi.org/10.1038/s41467-022-28151-9.
44. Sadati, M., Taheri Qazvini, N., Krishnan, R., Park, C.Y., and Fredberg, J.J. (2013). Collective migration and cell jamming. Differentiation. *86*, 121–125. https://doi.org/10.1016/j.diff.2013.02.005.
45. Cammarota, C., Dawney, N.S., Bellomio, P.M., Jüng, M., Fletcher, A.G., Finegan, T.M., and Bergstralh, D.T. (2024). The mechanical influence of densification on epithelial architecture. PLoS Comput. Biol. *20*, e1012001. https://doi.org/10.1371/journal.pcbi.1012001.
46. Fanning, A.S., Jameson, B.J., Jesaitis, L.A., and Anderson, J.M. (1998). The tight junction protein ZO-1 establishes a link between the transmembrane protein occludin and the actin cytoskeleton. J. Biol. Chem. *273*, 29745–29753. https://doi.org/10.1074/jbc.273.45.29745.
47. Haas, A.J., Zihni, C., Krug, S.M., Maraspini, R., Otani, T., Furuse, M., Honigmann, A., Balda, M.S., and Matter, K. (2022). ZO-1 Guides Tight Junction Assembly and Epithelial Morphogenesis via Cytoskeletal Tension-Dependent and -Independent Functions. Cells *11*, 3775. https://doi.org/10.3390/cells11233775.
48. Haas, A.J., Zihni, C., Ruppel, A., Hartmann, C., Ebnet, K., Tada, M., Balda, M.S., and Matter, K. (2020). Interplay between Extracellular Matrix Stiffness and JAM-A Regulates Mechanical Load on ZO-1 and Tight Junction Assembly. Cell Rep. *32*, 107924. https://doi.org/10.1016/j.celrep.2020.107924.
49. Jain, S., Cachoux, V.M.L., Narayana, G.H.N.S., de Beco, S., D'Alessandro, J., Cellerin, V., Chen, T., Heuzé, M.L., Marcq, P., Mège, R.M., et al. (2020). The role of single cell mechanical behavior and polarity in driving collective cell migration. Nat. Phys. *16*, 802–809. https://doi.org/10.1038/s41567-020-0875-z.
50. Corti, S., Bonjean, R., Legier, T., Rattier, D., Melon, C., Salin, P., Toso, E.A., Kyba, M., Kerkerian-Le Goff, L., Maina, F., and Dono, R. (2021). Enhanced differentiation of human induced pluripotent stem cells toward the midbrain dopaminergic neuron lineage through GLYPICAN-4 downregulation. Stem Cells Transl. Med. *10*, 725–742. https://doi.org/10.1002/sctm.20-0177.
51. Musah, S., Wrighton, P.J., Zaltsman, Y., Zhong, X., Zorn, S., Parlato, M.B., Hsiao, C., Palecek, S.P., Chang, Q., Murphy, W.L., and Kiessling, L.L. (2014). Substratum-induced differentiation of human pluripotent stem cells reveals the coactivator YAP is a potent regulator of neuronal specification. Proc. Natl. Acad. Sci. USA *111*, 13805–13810. https://doi.org/10.1073/pnas.1415330111.
52. Gutierrez, E., Tkachenko, E., Besser, A., Sundd, P., Ley, K., Danuser, G., Ginsberg, M.H., and Groisman, A. (2011). High refractive index silicone gels for simultaneous total internal reflection fluorescence and traction force microscopy of adherent cells. PLoS One *6*, e23807. https://doi.org/10.1371/journal.pone.0023807.
53. Lee, K., Elliott, H.L., Oak, Y., Zee, C.T., Groisman, A., Tytell, J.D., and Danuser, G. (2015). Functional hierarchy of redundant actin assembly factors revealed by fine-grained registration of intrinsic image fluctuations. Cell Syst. *1*, 37–50. https://doi.org/10.1016/j.cels.2015.07.001.
54. Li, D., Colin-York, H., Barbieri, L., Javanmardi, Y., Guo, Y., Korobchevskaya, K., Moeendarbary, E., Li, D., and Fritzsche, M. (2021). Astigmatic traction force microscopy (aTFM). Nat. Commun. *12*, 2168. https://doi.org/10.1038/s41467-021-22376-w.
55. Barai, A., Das, A., and Sen, S. (2021). Measuring microenvironment-tuned nuclear stiffness of cancer cells with atomic force microscopy. STAR Protoc. *2*, 100296. https://doi.org/10.1016/j.xpro.2021.100296.
56. Trappmann, B., Gautrot, J.E., Connelly, J.T., Strange, D.G.T., Li, Y., Oyen, M.L., Cohen Stuart, M.A., Boehm, H., Li, B., Vogel, V., et al. (2012). Extracellular-matrix tethering regulates stem-cell fate. Nat. Mater. *11*, 642–649. https://doi.org/10.1038/nmat3339.
57. Wen, J.H., Vincent, L.G., Fuhrmann, A., Choi, Y.S., Hribar, K.C., Taylor-Weiner, H., Chen, S., and Engler, A.J. (2014). Interplay of matrix stiffness and protein tethering in stem cell differentiation. Nat. Mater. *13*, 979–987. https://doi.org/10.1038/nmat4051.
58. Kim, J., Magli, A., Chan, S.S.K., Oliveira, V.K.P., Wu, J., Darabi, R., Kyba, M., and Perlingeiro, R.C.R. (2017). Expansion and Purification Are Critical for the Therapeutic Application of Pluripotent Stem Cell-Derived Myogenic Progenitors. Stem Cell Rep. *9*, 12–22. https://doi.org/10.1016/j.stemcr.2017.04.022.
59. Serra-Picamal, X., Conte, V., Vincent, R., Anon, E., Tambe, D.T., Bazellieres, E., Butler, J.P., Fredberg, J.J., and Trepat, X. (2012). Mechanical waves during tissue expansion. Nat. Phys. *8*, 628–634. https://doi.org/10.1038/Nphys2355.
60. Sader, J.E., Chon, J.W.M., and Mulvaney, P. (1999). Calibration of rectangular atomic force microscope cantilevers. Rev. Sci. Instrum. *70*, 3967–3969. https://doi.org/10.1063/1.1150021.
61. Oliver, W., and Pharr, G. (2004). Measurement of hardness and elastic modulus by instrumented indentation: Advances in understanding and refinements to methodology. J. Mater. Res. *19*, 3–20.
62. Olivier, W.C., and Pharr, G. (1992). An improved technique for determining hardness and elastic modulus using load and displacement sensing indentation experiments. J. Mater. Res. *7*, 1564–1583.
63. Schindelin, J., Arganda-Carreras, I., Frise, E., Kaynig, V., Longair, M., Pietzsch, T., Preibisch, S., Rueden, C., Saalfeld, S., Schmid, B., et al. (2012). Fiji: an open-source platform for biological-image analysis. Nat. Methods *9*, 676–682. https://doi.org/10.1038/Nmeth.2019.
64. Schmidt, U., Weigert, M., Broaddus, C., and Myers, G. (2018). Cell Detection with Star-Convex Polygons. In Medical Image Computing and Computer Assisted Intervention - Miccai 2018, Pt Ii 11071 (xxx), pp. 265–273. https://doi.org/10.1007/978-3-030-00934-2_30.
65. Stringer, C., Wang, T., Michaelos, M., and Pachitariu, M. (2021). Cellpose: a generalist algorithm for cellular segmentation. Nat. Methods *18*, 100–106. https://doi.org/10.1038/s41592-020-01018-x.
66. Aigouy, B., Umetsu, D., and Eaton, S. (2016). Segmentation and Quantitative Analysis of Epithelial Tissues. Methods Mol. Biol. *1478*, 227–239. https://doi.org/10.1007/978-1-4939-6371-3_13.

## STAR★METHODS

### KEY RESOURCES TABLE

| REAGENT or RESOURCE | SOURCE | IDENTIFIER |
|---|---|---|
| Antibodies | | |
| Goat anti-T-Brachyury (BRA, 1/80) | R&D Systems | 967332; RRID: AB_2200235 |
| Mouse anti-Zona Occludens 1 (ZO1, 1/500) | Invitrogen | 33–9100; RRID: AB_2533147 |
| Goat anti-SOX17 (1/80) | R&D Systems | 967330; RRID: AB_355060 |
| Mouse anti-OCT4 (1/400) | Santa Cruz Biotechnology | 5272; RRID: AB_628051 |
| Rabbit anti-NANOG (1/200) | Cell Signaling Technology | 4903; RRID: AB_10559205 |
| Rat anti-SOX2 (1/1000) | Invitrogen | 14-9811-32; RRID: AB_11219471 |
| Rabbit anti-ECAD (1/200) | Cell Signaling Technology | 3195; RRID: AB_2291471 |
| Chemicals, peptides, and recombinant proteins | | |
| DAPI | Invitrogen | D3571 |
| Activin A | R&D | 338-AC |
| ROCK inhibitor | Tocris | 1254 |
| PDMS (Sylgard 184) | Dow Corning | DC184–1.1 |
| QGel 920 | CHT Silicones | QGel 920 |
| Phalloidin ifluor 647 | ABCAM | AB176759 |
| Acrylamide | Bio-Rad | 1010140 |
| Bis-acrylamide | Bio-Rad | 1610142 |
| Matrigel | Corning | BV 354277 |
| Fluorescent beads | ThermoFisher Scientific | F8816 |
| Experimental models: cell lines | | |
| WT 029 Human induced pluripotent stem cells (hiPSCs) | University of Minnesota, MN | RRID:CVCL_VF55 |
| Software and algorithms | | |
| ZEN, version 3.4 | Zeiss | RRID: SCR_013672 |
| MATLAB, version R2023a | Mathworks | RRID: SCR_001622 |
| FIJI, version 2.14.0 | NIH | RRID: SCR_002285 |
| Prism, version 8.4.3 | GraphPad | RRID: SCR_002798 |
| FIJI StarDist Plugin | Max Planck Institute of Molecular Cell Biology and Genetics | NA |
| Cellpose, version 2.0 | Janelia research campus, VA | RRID: SCR_021716 |
| Tissue Analyzer | Aix-Marseille Université | NA |
| Other | | |
| Table Top Spin Coater POLOS SPIN150i | SPS | 41096 |
| Plasma cleaner | Harrick Plasma | PDC-002 |
| AFM | NT-MDT | NTEGRA-NTMDT |
| AFM tips | Nanosensors | CONT-Silicon-SPM-Sensor<br>PPP-PMR-Silicon Sensor |

## RESOURCE AVAILABILITY

### Lead contact

Further information and requests for resources and reagents should be directed to and will be fulfilled by Dr. Rosanna Dono (rosanna.dono@univ-amu.fr).

### Materials availability

This study did not generate new unique reagents.

### Data and code availability

- Data: All data reported in this paper will be shared by the lead contact upon request.
- Code: This paper does not report original code.
- Any additional information required to reanalyze the data reported in this paper is available from the lead contact upon request.

## EXPERIMENTAL MODEL AND STUDY PARTICIPANT DETAILS

### Cells and culture conditions

WT 029 hiPSCs were courtesy of Michael Kyba.[58] These are human induced pluripotent stem cells reprogrammed from mail somatic cells of an adult male. This material has been characterized by the NHLBI Progenitor Cell Biology Consortium (PCBC). HiPSCs were maintained on tissue culture-treated plastic, coated with Matrigel (BV 354277, Corning) according to supplier recommendations, in mTeSR1 medium (85850, Stemcell Technologies) supplemented with 1% Penicillin/Streptomycin cocktail (15140122, Invitrogen), and maintained in a humidified 37°C incubator with 5% $CO_2$. Medium was changed every 24 h, and cell cultures were dissociated using Accumax (SCR006, Millipore) and passaged 1/10 ad-hoc prior to confluency, approximately every 3–4 days. Media were supplemented with 10 μM ROCK inhibitor (1254, Tocris) in the 24 h following passage to facilitate cell adhesion and survival. All experiments described were performed by using different batches of WT 029 hiPSCs, from which we did not observe significant variance in iPSC cultures and differentiation efficiency. The cell lines were regularly tested for mycoplasma contamination.

## METHOD DETAILS

### Gel fabrication

PDMS and QGel silicones (Sylgard 184, Dow Corning; QGel 920, CHT Silicones) were both fabricated by mixing each base with its respective cross-linker solution. For each gel, the two solutions were mixed and degassed for 15 min 100 μL of the mixture was spin-coated onto #1.5 round coverslips (170 μm in thickness, 13 mm in diameter) at 1,200 rpm for 60 s. Gels were cured, i.e., reticulated, by overnight incubation at 60°C. Where appropriate, gel hydrophobicity was reversed to hydrophilicity via a 30-s plasma activation.

PA hydrogels were prepared by adapting previously described protocols.[59] Gel binding on the same glass coverslips as for PDMS gels was facilitated by activating the glass surface using a 1:1:14 solution of acetic acid (695092, Sigma)/bind-silane (10700467, VWR)/ethanol. The coverslips were washed twice with ethanol and air-dried for 10 min. Acrylamide and bis-acrylamide (1010140/1610142, Bio-Rad) were mixed in phosphate-buffered saline (PBS) at ratios corresponding to the desired stiffnesses. The polymerization reaction was catalyzed by adding 0.5% ammonium persulfate (A3678, Sigma) and 0.1% TEMED (T9281, Sigma). Before polymerization could occur, 10-μL drops were quickly added (coated with hydrophobic RAIN-X) and the drops were covered with the activated coverslips. PA hydrogels were left to polymerize for ~30 min, then washed three times with PBS. Hydrogels were then activated by 10-min incubation with 0.5 mg/mL Sulfo-SANPAH (22589, ThermoFisher Scientific) in MilliQ water under 365-nm UV light to facilitate Matrigel binding. After activation, gels were washed three times with PBS.

Prior to cell seeding, all substrates (including glass) were functionalized using Matrigel (BV 354277, Corning) according to manufacturer recommendation.

### Gel compositions and corresponding Young's moduli

The Young's moduli and standard deviations are respectively the weighted average and weighted standard deviations calculated from the N measurements (the inverse variance weighting was used to minimize the uncertainty). Note that we were not able to measure the softest QGel, but we expect from its composition to be softer than the 1.9 kPa QGel. The three gels' stiffnesses are compared to those of tissues in the schematics shown in Figure S6C.

| Gel type/Young's modulus | Standard deviation | Number of measurements | Composition | |
|---|---|---|---|---|
| PDMS | | | Base % | Cross-linker % |
| 2.18 MPa | 0.213 MPa | 33 | 90 | 10 |
| 77.6 kPa | 13.3 kPa | 36 | 98 | 2 |
| PA | | | Acrylamide % | Bis-acrylamide % |
| 32.1 kPa | 9.47 kPa | 36 | 12 | 0.2824 |
| 25.1 kPa | 5.08 kPa | 36 | 10 | 0.282 |

(*Continued on next page*)

*Continued*

| Gel type/Young's modulus | Standard deviation | Number of measurements | Composition | |
|---|---|---|---|---|
| PDMS | | | Base % | Cross-linker % |
| 11.6 kPa | 1.91 kPa | 51 | 7.464 | 0.16 |
| 4.07 kPa | 1.42 kPa | 44 | 5.488 | 0.05 |
| 2.15 kPa | 0.512 kPa | 35 | 3 | 0.06 |
| QGel | | | Solution A % | Solution B % |
| 31.2 kPa | 2.5 kPa | 23 | 33 | 67 |
| 1.9 kPa | 0.19 kPa | 24 | 40 | 60 |
| <1.9 kPa | – | – | 56 | 44 |

## Atomic force microscopy

Atomic Force Microscopy (AFM, NTEGRA-NTMDT) was used to measure the gel substrate roughness and Young's modulus.

### *Substrate roughness*

The surface roughness of substrates was measured using AFM in tapping mode. A PPP-FMR-Silicon probe (Nanosensors) was used, with a stiffness of 0.5–9.5 N/m and a resonance frequency of 60 Hz. Regions of 10 × 10 $\mu m^2$ were scanned and the average roughness was measured.

### *Substrate stiffness*

Nanoindentation experiments were performed using AFM in contact mode, by controlling the displacement of the piezoelectric element in the direction perpendicular to the surface and the time rate required to perform this displacement. The deflection of the cantilever was continuously measured during loading and unloading from the sample surface (typical loading/unloading curves are displayed in Figures S6A and S6B). In all experiments, the same type of probe, with low stiffness (<0.5 N/m), was used: CONT-Silicon –SPM-Sensor with a colloidal particle of diameter 6.62 $\mu m \pm 10\%$ as indicated by the manufacturer (Nanosensors). The probe's cantilever stiffness was measured using the Sader method.[60] Cantilever parameters were measured experimentally using the AFM setup (Resonance frequency and Quality factor) and optical microscopy (Width and Length). A total of four probes were used in the whole set of stiffness measurement experiments.

### *Cantilever parameters of AFM probes*

Prior to experiments, AFM probes were cleaned in acetone, and exposed for 30 s to oxygen plasma. To reduce a strong attractive interaction between the tip and the samples, the tips were functionalized with trimethoxymethylsilane, making their surface hydrophobic. Similarly, all experiments were performed in water to avoid capillary forces. For each set of measurements, cantilever sensitivity, i.e., deflection versus piezoelectric element z-displacement, was determined by performing a force-distance measurement on a hard silicon sample and further used to normalize the data curves. Indentation measurements were performed at a rate 1 Hz and a maximum loading force of 10 nN was applied during loading.

| Probe | Resonance frequency [kHz] | Quality factor | Width [μm] | Length [μm] | Stiffness [N/m] |
|---|---|---|---|---|---|
| 1 | 14.25 | 61.56 | 47.6 | 454 | 0.217 |
| 2 | 18.64 | 84.96 | 47.6 | 450 | 0.417 |
| 3 | 18.63 | 88.90 | 46.0 | 448 | 0.437 |
| 4 | 18.60 | 78.32 | 49.3 | 450 | 0.413 |

### *Extraction of Young's modulus*

Young's moduli were extracted using the Oliver & Pharr method,[61,62] which is suitable for processing both purely elastic and viscoelastic behaviors. The Young's modulus is extracted from the value of the slope (S) at the beginning of the unloading curve. For an indenter with a spherical shape, the relation between S, the maximum force (F), the indentation depth (h), the final depth (after the indenter is fully unloaded) ($h_f$), and the indentation modulus (M) is expressed as.

$$S = \frac{dF}{dh} = 2.\sqrt{R}.M.(h - h_f)^{1/2} \text{ where } M = \left(\frac{1 - \nu_s^2}{E} - \frac{1 - \nu_i^2}{E_i}\right)^{-1}$$

where E and $E_i$ are the Young's modulus of the sample and the indenter respectively, and $\nu_s$ and $\nu_i$, the sample and indenter Poisson's coefficients respectively. $E_i$ was fixed at 150 MPa, $\nu_i$ at 0.3 and $\nu_s$ at 0.5.

### Adherence, pluripotency, organization, and differentiation assays

For cell adherence and organization experiments, hiPSCs were seeded at a density of 110,000 cells/cm$^2$ onto Matrigel-coated coverslips in mTeSR1 medium supplemented as described earlier. After 24 h, fresh media was added with the omission of ROCK inhibitor. After a further 24 h (48 h in total post-seeding), bright field images were taken for adherence assays, or cells were fixed for 10 min using 4% paraformaldehyde (PFA) in PBS and analyzed by immunocytochemistry for pluripotency and organization assays.

Differentiation experiments of hiPSCs into mesendoderm and definitive endoderm lineages were performed by following published protocols.[26] hiPSCs were seeded onto Matrigel-coated coverslips in mTeSR1 medium supplemented as described earlier, at densities of 110,000 and 50,000 cells/cm$^2$ for mesendoderm and definitive endoderm differentiation experiments, respectively. After 24 h, fresh medium was added with the omission of ROCK inhibitor. After a further 24 h (48 h in total post-seeding), medium was removed and cells were washed twice with RPMI medium (Invitrogen, ref. 21875034), followed by the addition of RPMI medium supplemented with 100 ng/mL Activin A (338-AC, R&D), while control groups were maintained in supplemented mTeSR1 medium. After a further 24 h (72 h in total post-seeding), cells were either fixed to analyze mesendoderm differentiation by immunocytochemistry, or further cultured in fresh RPMI supplemented with 100 ng/mL Activin A and 0.2% defined, heat-inactivated fetal bovine serum (FBS, SH30071.02E, Hyclone). After a further 24 h (96 h in total post-seeding), cells were fixed to analyze definitive endoderm differentiation by immunocytochemistry. Slight differences in the overall differentiation efficiency were most likely caused by the growth rate of the cells at the plating stage, independent from substrate stiffness. Time course differentiation experiments of hiPSCs into mesendoderm and definitive endoderm lineages were performed as above with a slight modification. Specifically, differentiation was started 24 or 48 h after ROCK inhibitor removal to initiate differentiation when the epithelial sheet is at different levels of ZO1 organization.

Note that the density chosen for cell plating (e.g.,110,000 and 50,000 cells/cm$^2$ see above) balances the need to have cells at a density sufficient to best initiate the differentiation program without becoming too confluent at the time of fixation, which would otherwise cause cell detachment and adversely affect cell behavior.

### Chemical rescue of epithelial integrity

For epithelial integrity rescue experiments, hiPSCs were seeded at 130,000 cells/cm$^2$ density on Matrigel-coated coverslips in mTeSR1 medium supplemented with ROCK inhibitor. After 6 h, ROCK inhibitor was removed and either control medium or medium supplemented with 5 μM of LPA was added. After a further 24 h (30 h in total post-seeding), cells were fixed and analyzed by immunocytochemistry. Given the shorter duration of this experiment compared to the differentiation experiments, this higher cell plating density was chosen to obtain cells with a comparable epithelial organization at the start of the experiment set up.

For differentiation experiments in rescued epithelia, hiPSCs were seeded at 110,000 cells/cm$^2$ density on Matrigel-coated coverslips in mTeSR1 medium supplemented with ROCK inhibitor. After 24 h, ROCK inhibitor was removed and media supplemented with 5 μM of LPA was added. After a further 24 h (48 h in total post-seeding), cells were fixed to analyze mesendoderm differentiation by immunocytochemistry.

### Timeline and schematics of experiments

To facilitate the understanding of the sequences of steps (cell seeding, change of medium, biochemical treatments, fixation for immunostaining) used for each type of experiments, the various timelines are shown in Figure S7.

### Immunocytochemistry

Following fixation, cells were washed three times with PBS. Cells were permeabilized in 0.3% Triton X-100 (108603, Millipore) in PBS for 10 min at room temperature and blocked with 3% bovine serum albumin (A9647, Sigma), 2% donkey serum (ab7475, Abcam), 0.3% Triton X-100 in PBS for 1 h at room temperature. Cells were incubated with primary antibodies in blocking solution at 4°C overnight, followed by four PBS washes. Cells were then incubated with appropriate secondary antibodies (1/500 Invitrogen) in blocking solution with DAPI (D3571, Invitrogen) and Phalloidin-iFluor647 (where applicable, ab176759, ABCAM) for 1 h at room temperature. Cells were then washed four times using 0.3% Triton X-100 in PBS, following which coverslips were rinsed twice in MilliQ water before mounting onto 1-mm thick glass slides using antifade mounting medium (P36930, Invitrogen).

### Microscopy

Bright field images were taken on a Nikon Eclipse TS100 microscope using a DinoEye Edge AM7025X camera. Immunofluorescence images were acquired with either a Zeiss Axio Imager M2 wide-field or a Zeiss LSM 880 confocal microscope, using ZEN (version 3.4). Live cell imaging was carried out using a Zeiss Axio Observer Z1 fitted with a custom-built 37°C 5% $CO_2$ chamber. Cells were observed using a 20× objective over 6-h time periods and with a 5-min interval between frames to balance maximizing data acquisition and resolution with minimizing phototoxic exposure in order to ensure authenticity of cell behavior.

## QUANTIFICATION AND STATISTICAL ANALYSIS

### Immunofluorescence quantification

For quantification of BRA-positive mesendoderm cells, the number of positive cells showing nuclear localization of the transcription factor BRA were automatically counted by the FIJI software[63] (version 2.14.0). BRA-positive cells were defined as those whose mean fluorescence intensity was above the 95$^{th}$ percentile of the mean BRA intensity in Activin A-negative control cells at the same time point and stiffness. DAPI staining was used to define nuclear areas and total cell numbers using the StarDist[64] plugin of the FIJI software. SOX17-positive definitive endoderm cells were identified using the FIJI plugin StarDist as above. For analysis of BRA-positive cells, at least 10 randomly selected frames of view were taken per condition, covering >2.23 mm$^2$ in total. N = from 3 to 7 paired replicates (specified for each individual figure). For analysis of SOX17-positive cells, at least 3 randomly selected frames of view were taken per condition, covering >21.2 mm$^2$ in total. $N$ = 4 unpaired replicates.

Quantification of BRA-positive mesendoderm cells in ZO1 organized versus disorganized areas was done by manually counting BRA-positive mesendoderm cells and DAPI positive nuclei in both areas using the FIJI software. From 2 to 3 randomly selected frames of view were taken per condition. $N$ = 3 unpaired replicates.

### Organization quantification

The Cellpose algorithm[65] (version 2.0) was used to identify cells fully bound by ZO1 contacts in ZO1 immunofluorescent images. Connected regions of fully ZO1-bound cells were classified as areas of epithelial organization. The percentage organization in each image was calculated as the percentage of the total frame of view covered by areas of epithelial organization.[36] At least 3 to 4 randomly selected frames of view were taken per condition, covering >5.28 mm$^2$ in total. $N$ = 4 to 6 ratio paired replicates (specified for each individual figure).

### Growth analysis

The confluency of cells in phase-contrast frames of time lapses was calculated using FIJI. Images were converted to binary images using automatic thresholds, and objects filtered according to a size minimum of 5000 px$^2$ (image calibration: 0.631 μm/px). The confluency at each time point was defined as the percentage of the frame of view taken up by objects.

### Motility analysis

Automatic thresholding in FIJI was used to identify cell areas in phase-contrast frames of time lapses, and non-cell areas were subtracted from frames. In time lapses of single cell growth, images were converted to binary images and objects were filtered according to a size minimum of 1000 px$^2$ (0.631 μm/px). In time lapses of cell growth within colonies, objects were filtered according to a size minimum of 5000 px$^2$. The 2D correlation coefficient is defined as $\frac{\sum_m\sum_n (A_{mn}-\overline{A})(B_{mn}-\overline{B})}{\sqrt{\left(\sum_m\sum_n (A_{mn}-\overline{A})^2\right)\left(\sum_m\sum_n (B_{mn}-\overline{B})^2\right)}}$, where $A$ and $B$ are $m \times n$ arrays with respective means $\overline{A}$ and $\overline{B}$. Reading each frame as an array, the 2D correlation coefficient was calculated for 72 pairs of successive frames using the inbuilt function corr2 in MATLAB software (R2023a version, Mathworks).

### Epithelial features: cell density and shape index

Images of hiPSC epithelia immunostained with ZO1 were segmented using the Tissue Analyzer algorithm[66] then processed using FIJI. The ZO1 segmentations were used to create a mask. The images of nuclei labeled with DAPI were filtered using the masks and the StarDist plugin was used to segment and count the nuclei in ZO1 organized regions. Conversely, the ZO1-positive masks were inverted to create ZO1-negative masks of disorganized regions and the same procedure was applied to count nuclei in disorganized regions. Nucleus counting was considered as a proxy for cell counting. Cell densities in organized and disorganized areas were then calculated using ImageJ, considering only images with sufficiently large organized/disorganized regions (practically, those passing a 10–90% organization filter). Surface area of ZO1 organized and disorganized areas were quantified and cell density was computed by diving the cell number by the surface area. At least 3 to 6 randomly selected frames of view were taken per condition, covering >1.31 mm$^2$ in total. $N$ = 4 unpaired replicates. The ZO1 segmentations were also used to calculate each cell's shape index, defined as $\frac{P}{\sqrt{A}}$, where $P$ is the cell perimeter and $A$ is the cell area.[43]

### Statistical analyses

All statistical analyses were performed using Prism software (8.4.3 version, GraphPad). Data are represented as mean ± SEM, and $p$ values show the results of a two-tailed t test (*, <0.05; **, <0.01; ***, <0.001). The number of replicates in *in vitro* measurements represents the number of gel-coated/glass coverslips tested. Where replicates were performed using cells of different batches, replicates were paired accordingly. ZO1 organization experiments were found to be particularly sensitive to cells' growth phase at the onset of experiments, and so replicates were ratio-paired. Statistical significance of cell motility was assessed by comparing 72 pairs of successive frames for each time lapse. Statistical significance of changes in cell density across substrates was assessed using a two-way ANOVA to isolate effects due to substrate from density differences between organized and disorganized areas.